Task 1.3
Contribution to Design Criteria for
Industrialized Masonry Vaults

Késio Palácio, Paulo B. Lourenço, Joaquim Barros

Report 03-DEC/E-10

The present research has been carried out under
contract GROW-1999-70420 "ISO-BRICK" from the European Commission

Date: March 2003
No. of Pages: 46

Keywords: design criteria, masonry vaults, arches

Escola de
Engenharia

Departamento de
Engenharia Civil

Universidade
do Minho

Azurém, 4800-085 Guimarães - Tel. +351 253 510 200 - Fax +351 253 510 217 - E-mail secG@civil.uminho.pt

Contents

Azurém, P – 4800-058 Guimarães Tel. +351 253 510200 • Fax +351 253 510217

1 Introduction

Masonry vaults are one of the most common structural forms present in the architectural heritage of almost all countries in the world. These structures are defined as structures in which the load bearing is clearly associated with the distribution of material in space. Masonry vaults can assume many different shapes, being the most common shapes shown in Figure 1.1.

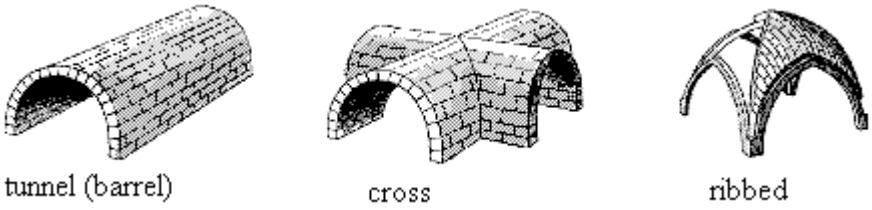

Figure 1.1 – Types of vaults

The vaulted structures are usually considered as an ideal system of arches. Clearly, barrel vaults can be understood as a set of parallel arches, each one beside the other, but also the other vaults, of more complex shape, can be generally outlined in a similar way, with a system of main arches that support secondary arches. It is noted that, in some cases, simplifications using ideal arched schemes lead to difficulties in justifying equilibrium, especially when the loads are not uniformly distributed, Giuriani, Gubana & Arenghi (2001). Therefore, true three-dimensional analysis and behavior is necessary for more complex cases.

Here, only a methodology for the analysis and design of (plane) arches is addressed. Since, in most cases, the analysis and design of vaults is possible using a subdivision into arches, the approach should be considered general. The standard techniques for simplified analysis and design criteria of vaults (=arches) include both elastic and plastic approaches.

The use of elastic and plastic approaches for the analysis and design of masonry vaults are discussed in the Chapter 2, only with respect to the application of a point load and a two-pinned arch, which has been the main focus of the vaults tested in the framework of the ISOBRICK project. Nevertheless, extension of the given formulation to other loading conditions is straightforward. Finally, Chapter 3 applies the proposed approaches to the vaults

Azurém, P – 4800-058 Guimarães Tel. +351 253 510200 • Fax +351 253 510217

tested in the framework of the ISOBRICK project, and Chapter 4 presents recommendations for practice.

Azurém, P – 4800-058 Guimarães Tel. +351 253 510200 • Fax +351 253 510217

2 Design Criteria for Vaults

An engineering structure has to satisfy many functional requirements. Two of the most important requirements are that the structure is strong enough to resist the applied loading (including its own weight) without collapsing, and that the structure is stiff enough not to deflect unduly under such loading. To achieve this functional requirement, the usual design procedures are based on the elastic behavior of the structure. On this basis, the strength of a structure is assessed from the observation or calculation of how close the structure is to yielding in any of its parts.

For materials and structures exhibiting plastic behavior, which normally includes arched structures, there is an alternative method of design called plastic method of design, or ultimate strength design. This method is based on the fact that structural elements cannot deflect indefinitely or collapse until a mechanism if formed. In the case of arches, beams or rigid frames, the requirement of a mechanism indicates that the full plastic moment *Mp* has developed at each of several critical sections. If it is assumed that the plastic moment acts at each such section, then the problem becomes statically determinate and the load corresponding to the collapse condition can be readily calculated.

Thus, this reports presents the design criteria for vaults, using both elastic and plastic analysis of arches, and compares the propose criteria with the experimental collapse loads obtained by Sarrablo (2002).

2.1 Elastic Design Formulation

The elastic formulation for curved members adopted here is based on the assumption that the cross-sectional dimensions of the member are small compared with the radius of curvature, so that the stresses can be calculated by formulas applicable for straight members. Additionally, given the fact that elastic analysis is addressed, the effect of deformations on the bending moments may be neglected and the principle of superposition is applicable.

The evaluation of the normal stresses σ in a cross-section of an arch, subjected to combined axial loading *N* and bending moment *M*, is given by the following equations:

Azurém, P – 4800-058 Guimarães Tel. +351 253 510200 • Fax +351 253 510217

Upper flange: $$\sigma_{top} = \frac{N}{A} + \frac{M}{I} \cdot c_{top} \quad (2.1a)$$

Lower flange: $$\sigma_{bot} = \frac{N}{A} + \frac{M}{I} \cdot c_{bot} \quad (2.1b)$$

Here, A and I are respectively the area and inertia of the cross-section, c is the distance of the extreme fiber to the center of gravity (c.g.) of the cross-section, and the subscripts *top* and *bot* indicate the upper and lower flanges respectively, see Figure 2.1.

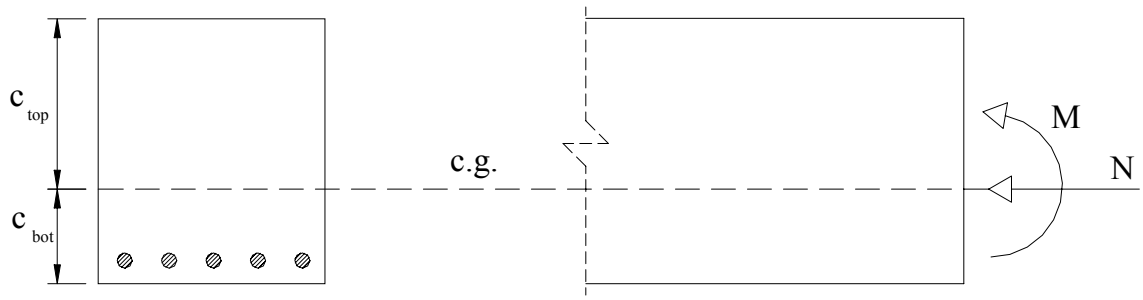

Figure 2.1– Cross-section area subjected to combined axial load and bending moment

The elastic analysis requires the calculation of normal stresses from the internal forces, which in this case are the axial force N and the bending moment M, and the comparison of these stresses with the maximum admissible stresses. The problem of the determination of the internal forces is addressed next.

2.1.1 Structural Analysis

The structural analysis for a two-pinned arch subjected to a single concentrated load P plus its own uniformly distributed weight q (see Figure 2.2) is developed here.

The shape of the arch is assumed parabolic instead of the original catenary shape adopted by Sarralbo (2002). This assumption simplifies the analysis to great extent because an explicit solution exists for the shape of the arch, in opposition with the implicit catenary formulation. Such simplification does not affect the results because parabolic and catenary are very similar shapes. For the catenary vaults of Sarralbo (2002), with a chord of 4.0 m and a rise of 1.0 m, the elevations of the half span of the arch are shown in Table 2.1, where a maximum error of 5% is found, with respect to the parabolic arch.

Azurém, P – 4800-058 Guimarães Tel. +351 253 510200 • Fax +351 253 510217

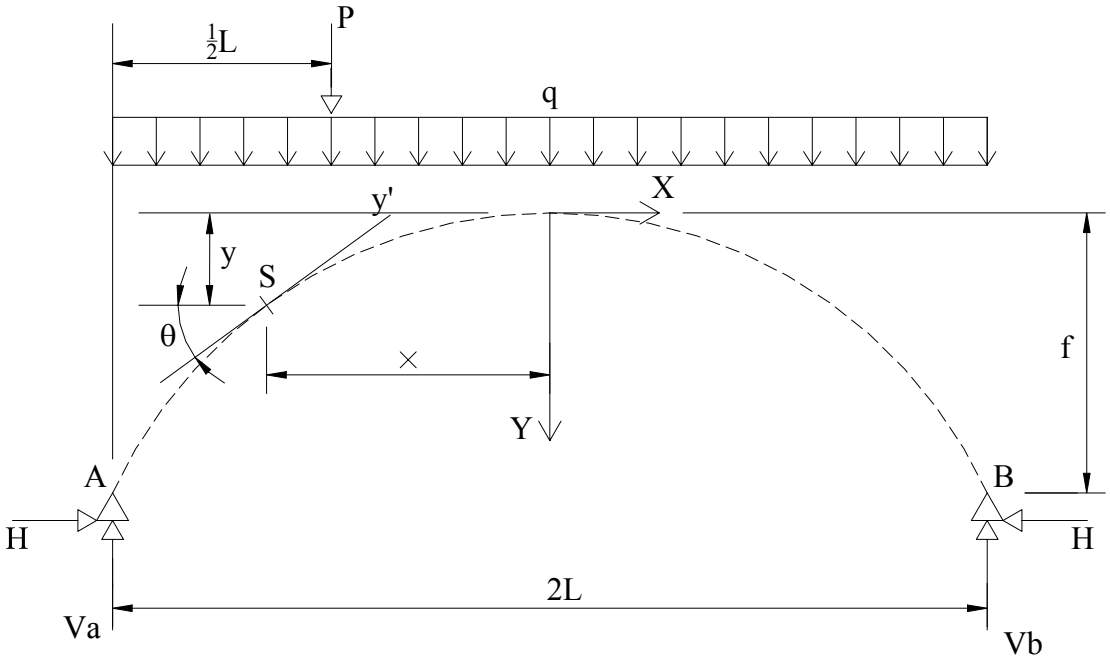

Figure 2.2 – Two-pinned arch submitted to a single concentrated load plus its own weight

Table 2.1 – Comparison between catenary and parabolic shapes

x(m)	0.0	0.2	0.4	0.6	0.8	1.0	1.2	1.4	1.6	1.8	2.0
Catenary shape (half span)											
y(m)	0.000	0.010	0.038	0.085	0.151	0.237	0.344	0.473	0.624	0.800	1.000
Parabolic shape (half span)											
y(m)	0.000	0.010	0.040	0.090	0.160	0.250	0.360	0.490	0.640	0.810	1.000
Error in elevation											
Error(%)	0.0	0.0	5.0	5.5	5.6	5.2	4.4	3.4	2.5	1.2	0.0

Here, it is noted that, for a span $2L$ (= 4.0 m) and a rise f (= 1.0 m), the shape of the vault is given by the following expressions:

Catenary shape: $$y = 2.1486 \cdot \cosh(0.4654x) - 2.1486 \quad (2.2a)$$

Parabolic shape: $$y = \frac{f}{L^2} x^2 \quad (2.2b)$$

From the strength of materials, see e.g. Rodriguez and Azcunaga (1980), the unknown hyperstatic reaction H may be determined by

Azurém, P – 4800-058 Guimarães Tel. +351 253 510200 • Fax +351 253 510217

$$H = \frac{\int_0^{2L} \frac{M_S\, y \cdot ds}{EI}}{\int_0^{2L} \frac{y^2 \cdot ds}{EI} + \int_0^{2L} \frac{ds}{EA}}, \tag{2.3}$$

where M_S is the bending moment, at section S, for a simply supported beam.

In Eq. (2.3), the terms (ds / I) and (ds / A) vary along the parabolic arch. However, their variations may be approximated using the secant assumption, where sec θ = 1 / cosθ. Thus, the following expressions are obtained, Rodriguez and Azcunaga (1980),

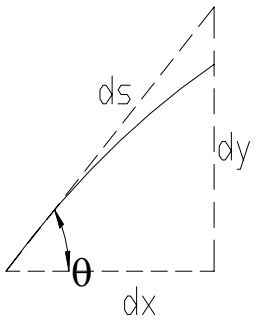

$$\begin{aligned} ds &= dx \cdot \sec\theta \\ I &= I_o \cdot \sec\theta \\ A &= A_o \cdot \sec\theta \end{aligned}, \tag{2.4}$$

where I_o and A_o are the values of inertia and area for the cross section, at the crown of the arch.

Therefore, introducing Eq. (2.4) in Eq. (2.3) and assuming that the Young's modulus E is constant throughout the arch, it is possible to obtain

$$H = \frac{\frac{1}{I_o}\int_0^{2L} M_S\, y dx}{\frac{1}{I_o}\int_0^{2L} y^2 dx + \frac{1}{A_o}\int_0^{2L} dx}. \tag{2.5}$$

The value of the bending moment M_S, at any section S of a beam having the same span as the arch, may be written as,

Azurém, P – 4800-058 Guimarães Tel. +351 253 510200 • Fax +351 253 510217

$$\begin{cases} M_S^{(1)} = \left(\frac{3}{4}P + qL\right)\cdot(x+L) - q\frac{(x+L)^2}{2}, & \text{for } -L \le x \le -\frac{L}{2} \\ M_S^{(2)} = \left(\frac{3}{4}P + qL\right)\cdot(x+L) - q\frac{(x+L)^2}{2} - P\cdot\left[(x+L) - \frac{L}{2}\right], & \text{for } -\frac{L}{2} \le x \le L \end{cases} \quad (2.6)$$

The solution of Eq. (2.5), replacing M_S according to Eq. (2.6) and assuming the parabolic shape of the arch, given by Eq. (2.2.b), results in the following:

Numerator

$$\frac{1}{I_O}\int_{-L}^{L} M_S \cdot y \cdot dx = \frac{1}{I_O}\left[\int_{-L}^{-L/2} M_S{}^{(1)} y dx + \int_{-L/2}^{L} M_S{}^{(2)} y dx\right] \quad (2.7a)$$

$$\int_{-L}^{-L/2} M_S{}^{(1)} \cdot y \cdot dx = \int_{-L}^{-L/2}\left[\left(\frac{3}{4}P + qL\right)\cdot(x+L) - q\frac{(x+L)^2}{2}\right]\cdot\frac{f}{L^2}x^2 \cdot dx = \frac{PL^2 f}{1024} - \frac{7qL^3 f}{3200} \quad (2.7b)$$

$$\int_{-L/2}^{L} M_S{}^{(2)} \cdot y \cdot dx = \int_{-L/2}^{L}\left\{\left(\frac{3}{4}P + qL\right)\cdot(x+L) - q\frac{(x+L)^2}{2} - P\cdot\left[(x+L) - \frac{L}{2}\right]\right\}\cdot \frac{f}{L^2}x^2 \cdot dx = \frac{241PL^2 f}{3072} + \frac{661qL^3 f}{9600} \quad (2.7c)$$

$$\frac{1}{I_O}\int_{-L}^{L} M_S \cdot y \cdot dx = \frac{61PL^2 f}{768 I_O} + \frac{qL^3 f}{15 I_O} \quad (2.7d)$$

Denominator

$$\frac{1}{I_o}\int_{-L}^{L} y^2 \cdot dx + \frac{1}{A_o}\int_{-L}^{L} dx = \frac{1}{I_o}\int_{-L}^{L}\left[\frac{4f}{L^2}\left(Lx - x^2\right)\right]^2 dx + \frac{1}{A_o}\int_{-L}^{L} dx = \frac{8Lf^2}{15 I_o} + \frac{L}{A_o} \quad (2.8)$$

Finally, introducing Eq. (2.7d) and Eq. (2.8) into Eq. (2.5), the value of the horizontal reaction of the arch, necessary for establishing the equations of the internal forces, can be calculated as,

Azurém, P – 4800-058 Guimarães Tel. +351 253 510200 • Fax +351 253 510217

$$H = \frac{\frac{61PL^2 f}{768I_o} + \frac{qL^3 f}{15I_o}}{\frac{8Lf^2}{15I_o} + \frac{L}{A_o}}. \tag{2.9}$$

Once the horizontal reaction H is determined, it is possible to calculate the axial force N and the bending moment M at any section S of the arch, as

For $-\mathrm{L} \le \mathrm{x} \le -\frac{\mathrm{L}}{2}$,

$$\begin{aligned} M_S(x,y)^1 &= V_A \cdot (x+L) - \frac{q \cdot (x+L)^2}{2} - H \cdot (f-y) \\ Ns(x,\theta)^1 &= q \cdot (x+L)\sin\theta - V_A \cdot \sin\theta - H \cdot \cos\theta \end{aligned} \tag{2.10}$$

For $-\frac{\mathrm{L}}{2} \le \mathrm{x} \le L$,

$$\begin{aligned} M_S(x,y)^2 &= V_A \cdot (x+L) - \frac{q \cdot (x+L)^2}{2} - \mathrm{P} \cdot \left[(\mathrm{x}+2) - \frac{\mathrm{L}}{2} \right] - H \cdot (f-y) \\ Ns(x,\theta)^2 &= q \cdot (x+L)\sin\theta - V_A \cdot \sin\theta - H \cdot \cos\theta \end{aligned}. \tag{2.11}$$

Here, V_A is the vertical reaction at support A (see Figure 2.2) and is given by

$$V_A = \frac{3}{4}P + qL. \tag{2.12}$$

Thus, with the internal forces N and M calculated throughout the span of the arch, one may compute the stresses σ_{bot} and σ_{top} at any section of the arch and compare these with the maximum admissible stresses.

2.2 Plastic Design Formulation

As referred in the introduction, it is possible to use the plastic method of design, which is based on the assumptions of the plasticity theory, to evaluate the collapse load for arches. There are two common methods of plastic design, namely the static method and the kinematic

Azurém, P – 4800-058 Guimarães Tel. +351 253 510200 • Fax +351 253 510217

method. Both plastic approaches will be employed here to determine the collapse load of a two-pinned arch subjected to a point load *P*.

The self-weight of the arch will not be taken into account in order to simplify the analysis. It is stressed that this assumption does not affect the results significantly because the self-weight of the arch is much lower than the collapse load, as it will be shown in Chapter 3.

2.2.1 Static Approach

To apply the static approach for arch structures, the concept of line-of-thrust is particularly appealing. The line-of-thrust is the path followed by the resultant of the forces acting on the cross-section of the arch, over its full span. For the case of a two-pinned arch, the line-of-thrust is sketched in Figure 2.3, together with additional symbols that will be used in the derivation.

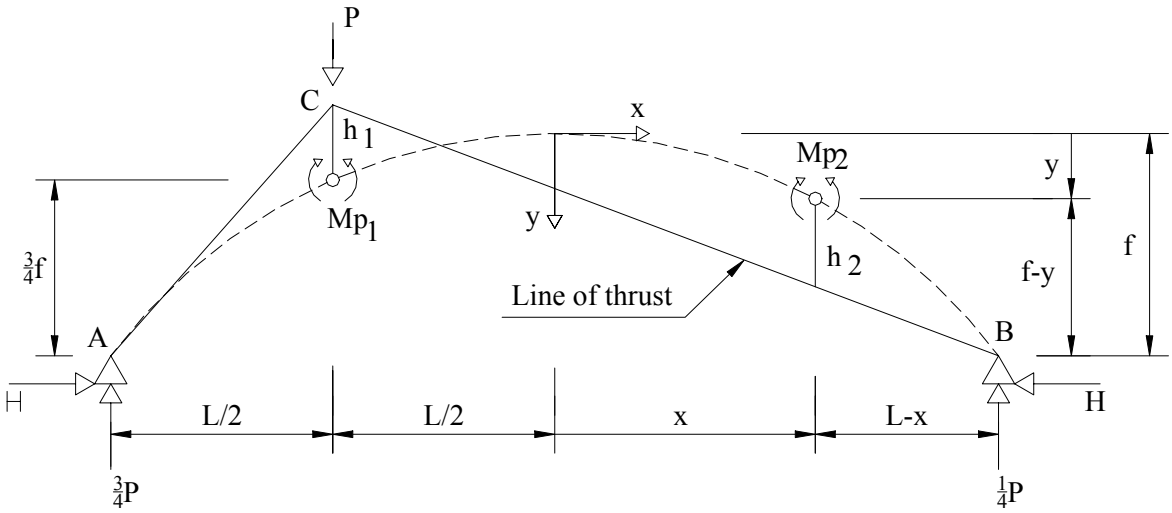

Figure 2.3 – Line-of-thrust for a two-pinned arch carrying a single point load *P*.

For a two-pinned arch, the conditions of failure depend upon the position of loads. For a non-symmetrical application of loads, which is the condition presented in Figure 2.3, two plastic hinges will be formed at collapse, associated with plastic moments Mp_1 and Mp_2. The location of the first hinge is defined by the application of the point load, whereas the location of the second hinge represents a singular point so that $dP / dx = 0$. Here, the horizontal and vertical distance from the crown are given by *x* and *y*, respectively. The values of the plastic moments can be found by using a basic property of an arch, which is based on equilibrium

Azurém, P – 4800-058 Guimarães Tel. +351 253 510200 • Fax +351 253 510217

and holds both for elastic or plastic analysis: the vertical distance between the line-of-thrust and the center line of the arch, multiplied by the horizontal component of the thrust at the abutment, gives the value of the bending moment at any section. Thus,

$$Mp_1 = H \cdot h_1 \quad . \tag{2.13}$$

$$Mp_2 = H \cdot h_2 \tag{2.14}$$

Eqs. (2.13) and (2.14) may also be written as,

$$Mp_1 = \frac{3}{4} P \cdot \frac{L}{2} - H \cdot \frac{3}{4} f \tag{2.15}$$

$$Mp_2 = -\frac{P}{4} \cdot (L - x) + H \cdot (f - y), \tag{2.16}$$

where $y = \frac{f}{L^2} \cdot x^2$.

Introducing Eq. (2.14) in Eq. (2.16), it is possible to obtain the value of *P*, given by

$$P = \frac{4H}{L - x} \cdot (f - y - h_2) \tag{2.17a}$$

$$P = 4H \frac{f}{L^2} \cdot (L + x) - \frac{H \cdot h_2}{L - x} . \tag{2.17b}$$

By using eq.(2.14), eq. (2.17b) may be written as function of Mp_2,

$$P = 4Mp_2 \left[\frac{f}{h_2 L^2} \cdot (L + x) - \frac{1}{L - x} \right] \tag{2.17c}$$

The distance *x* can be found by taking the derivative of *P* with respect to *x* and setting it equal to zero, as defined before. Thus,

$$\frac{dP}{dx} = 4Mp_2 \cdot \left[\frac{f}{h_2 L^2} - \frac{1}{(L - x)^2} \right] = 0 \tag{2.18}$$

Azurém, P – 4800-058 Guimarães Tel. +351 253 510200 • Fax +351 253 510217

$$x = L \cdot \left(1 - \sqrt{\frac{h_2}{f}}\right) \quad . \tag{2.19}$$

The value of h_2 can be obtained directly from Figure 2.3 as

$$h_2 = y - \frac{2 \cdot (3f + h_1) \cdot (L - x)}{6 \cdot L} \ . \tag{2.20}$$

Using Eqs. (2.20), (2.13) and (2.14), it is possible to find the value of h_2 for given values of Mp_1 and Mp_2. For example, if Mp_1 equals Mp_2, then $h_1 = h_2 = h$. Therefore, Eq. (2.20) reads,

$$h = y - \frac{2 \cdot (3f + h) \cdot (L - x)}{6 \cdot L} . \tag{2.21}$$

Introducing the expression of a parabolic arch and rearranging the expression, it is possible to obtain

$$-6f \cdot x^2 + (3fL + 4Lh) \cdot x + L^2 (3f - 10h) = 0 \ . \tag{2.22}$$

Eq. (2.22) is a quadratic equation with a determinant D given by

$$D = L^2 \cdot (81f^2 - 216fh + 16h^2) . \tag{2.23}$$

In order to obtain real roots, the determinant D must be equal or greater than zero, meaning that following interval is obtained

$$\{h \in \Re \quad \text{if} \quad h \le 0.386f \ \text{ or } \ \text{h} \ge 13.114\text{f}\} . \tag{2.24}$$

As the value of h must be such that $0 < h < f$, it is straightforward to conclude that the maximum value for h is $0.386f$. Replacing h in Eq. (2.19), the obtained value of x is equal to $0.379L$.

Azurém, P – 4800-058 Guimarães Tel. +351 253 510200 • Fax +351 253 510217

Similar elaboration gives the values shown in Table 2.2, for different values of Mp_1 and Mp_2, obtained using Eqs. (2.20) and (2.19). Once the value of the distance x is known, the value of the ultimate P_u can be obtained from eq. (2.17c).

Table 2.2 – Values of the location x for the second plastic hinge and of the ultimate load P_u, for given values of Mp_1 and Mp_2

Mp_1	Mp_2	h_2	x	P_u
Mp	0	0	L	∞
Mp	Mp	0.386f	0.379L	15.70Mp/L
Mp	0.5Mp	0.301f	0.451L	8.73Mp/L

The condition of $Mp_1 = Mp$ and $Mp_2 = 0$ in Table 2.2, means that the second plastic hinge coincides with the right support B. This is a limit theoretical solution because a two-pinned arch with a load at one fourth of its span has commonly two plastic hinge formations. The given data ($Mp_2 = 0$) is questionable, as the self-weight of the structure will induce an axial load in arch, meaning that Mp_2 is always different than zero.

2.2.2 Kinematic Approach

Now, the principle of virtual work will be used to carry out the plastic analysis, for the same structure, as given in the preceding sections. Obviously, the results will be the same as in Section 2.2.1, but the approach can be of interest for more complex loading or structures. It is for the practitioner to decide which technique is more appealing to solve a given problem, for which an explicit solution does not exist.

To apply the kinematic approach, it is necessary to, firstly, define an admissible collapse mechanism. As pointed out in the previous section, failure of the arch occurs once two plastic hinges are formed. Therefore, it is possible to construct the collapse mechanism shown in Figure 2.4.

Azurém, P – 4800-058 Guimarães Tel. +351 253 510200 • Fax +351 253 510217

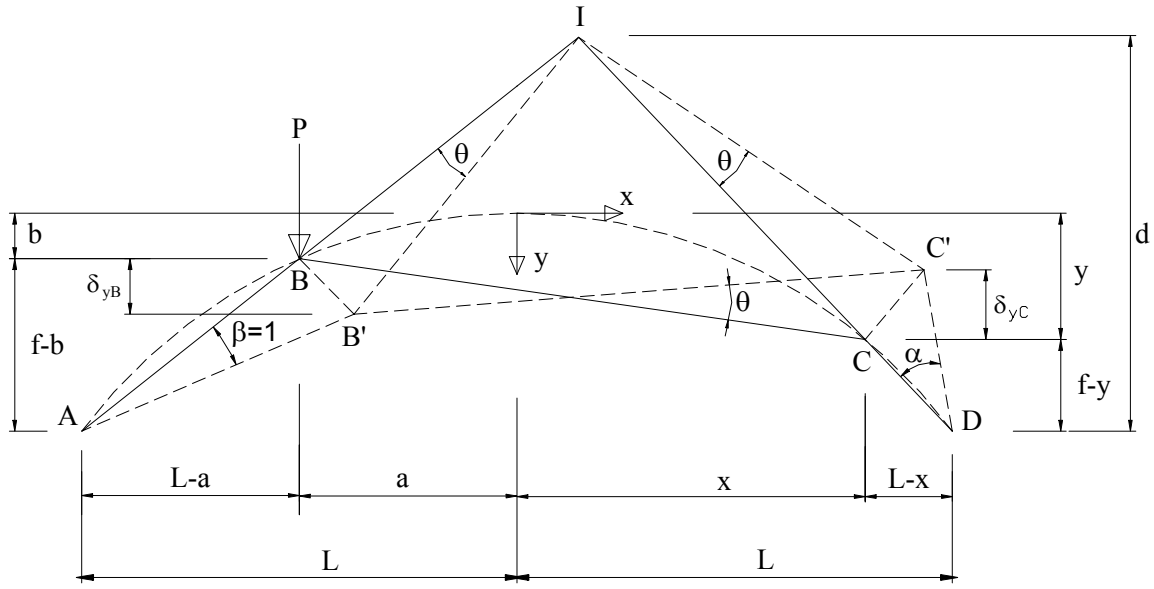

Figure 2.4 – Collapse mechanism for the arch carrying a single load *P*

The virtual work principle states that the external work δW_{ext} produced in any virtual deformation must be equal to the internal work δW_{int}, or

$$\delta W_{ext} = \delta W_{\text{int}}\,, \tag{2.25}$$

which can be recast as

$$P(L-a)\beta = Mp_1 \cdot (1+\theta) + Mp_2 \cdot (\alpha+\theta) \tag{2.26}$$

or

$$P = \frac{Mp_1}{L-a} \cdot (1+\theta) + \frac{Mp_2}{L-a} \cdot (\alpha+\theta). \tag{2.27}$$

Here, the rotation angles α, β and θ of the rigid parts of the arch are defined in Figure 2.4 and the vertical displacement of force P is given by $(L - a).\beta$. To define the virtual deformed configuration, and for the sake of simplicity, the angle β was assumed equal to the unit value.

In order to solve Eq. (2.27), it is necessary to calculate the values of the remaining angles α and θ, that is, the relations that describe how these angles vary as a function of the location of second plastic hinge. This can be carried out as follows:

Azurém, P – 4800-058 Guimarães Tel. +351 253 510200 • Fax +351 253 510217

1) Calculation of angle θ

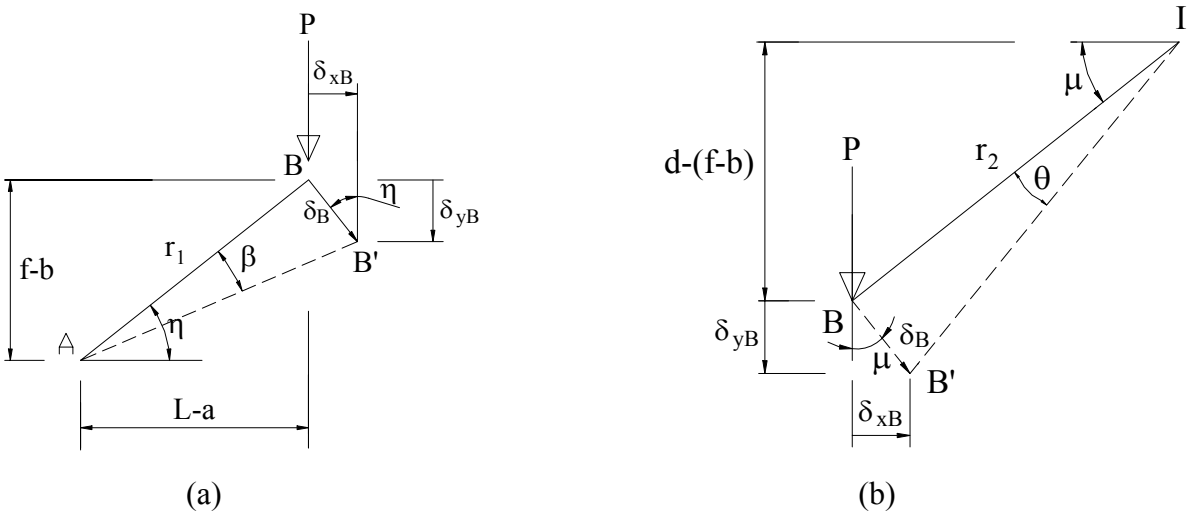

Figure 2.5 - Rotation and nodal displacement for bars AB and BI

From the deformed configurations of bar AB (rotation β) and BI (rotation θ), see Figure 2.5, it is possible to obtain:

From triangle ABB' one may get the following relations,

$$\frac{f-b}{r_1} = \sin\eta \tag{2.28}$$

$$\frac{\delta_B}{r_1} = \tan\beta \approx \beta \;\Rightarrow\; \delta_B = \mathrm{r}_1 \cdot \beta \tag{2.29}$$

$$\delta_{xB} = \delta_B \sin\eta = r_1\beta \cdot \frac{f-b}{r_1} = (f-b)\beta \tag{2.30}$$

Similarly for triangle BIB',

$$\frac{d-(f-d)}{r_2} = sen\mu \tag{2.31}$$

$$\frac{\delta_B}{r_2} = \tan\theta \approx \theta \;\Rightarrow\; \delta_B = \mathrm{r}_2 \cdot \theta \tag{2.32}$$

Azurém, P – 4800-058 Guimarães Tel. +351 253 510200 • Fax +351 253 510217

$$\delta_{xB} = \delta_B \sin\mu = r_2\theta \cdot \frac{d-(f-b)}{r_2} = d-(f-b)\cdot\theta \tag{2.33}$$

From Eqs. (2.30, 2.33), it is straightforward to obtain

$$\theta = \frac{f-b}{d-(f-b)}. \tag{2.34}$$

2) Calculation of angle α

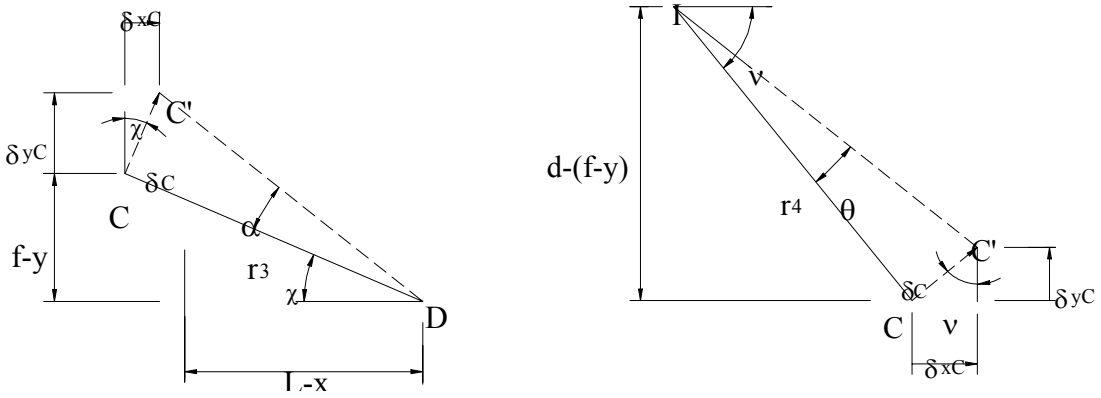

(a) (b)

Figure 2.6 - Rotation and nodal displacement for bars CD and CI

From the deformed configurations of bars DC (rotation α) and CI (rotation θ), see Figure 2.6, it is possible to obtain:

From triangle DCC' one may get the following relations,

$$\frac{f-y}{r_3} = \sin\chi \tag{2.35}$$

$$\frac{\delta_C}{r_3} = \tan\beta \approx \beta \;\Rightarrow\; \delta_C = \mathrm{r}_3 \cdot \alpha \tag{2.36}$$

$$\delta_{xC} = \delta_C \sin\chi = r_3\alpha \cdot \frac{f-y}{r_3} = (f-y)\cdot\alpha \tag{2.37}$$

Azurém, P – 4800-058 Guimarães Tel. +351 253 510200 • Fax +351 253 510217

Similarly for triangle CIC',

$$\frac{d-(f-y)}{r_4}=\sin\nu \tag{2.38}$$

$$\frac{\delta_C}{r_4}=\tan\theta\approx\theta\ \Rightarrow\ \delta_C=\mathrm{r}_4\cdot\theta \tag{2.39}$$

$$\delta_{xC}=\delta_C\sin\nu=r_4\theta\cdot\frac{d-(f-b)}{r_4}=d-(f-y)\cdot\theta \tag{2.40}$$

From Eqs. (2.34, 2.40), it is straightforward to obtain

$$\alpha=\frac{[d-(f-y)]}{(f-y)}\cdot\theta\,. \tag{2.41}$$

Introducing Eq. (2.34) in (2.41), the value of α reads

$$\alpha=\frac{d-(f-y)}{(f-y)}\cdot\frac{(f-b)}{d-(f-b)}\,. \tag{2.42}$$

Here, the elevation of the center of rotation *I*, given by *d*, is unknown, being calculated from the similarity of triangles, with the help of Figure 2.7.

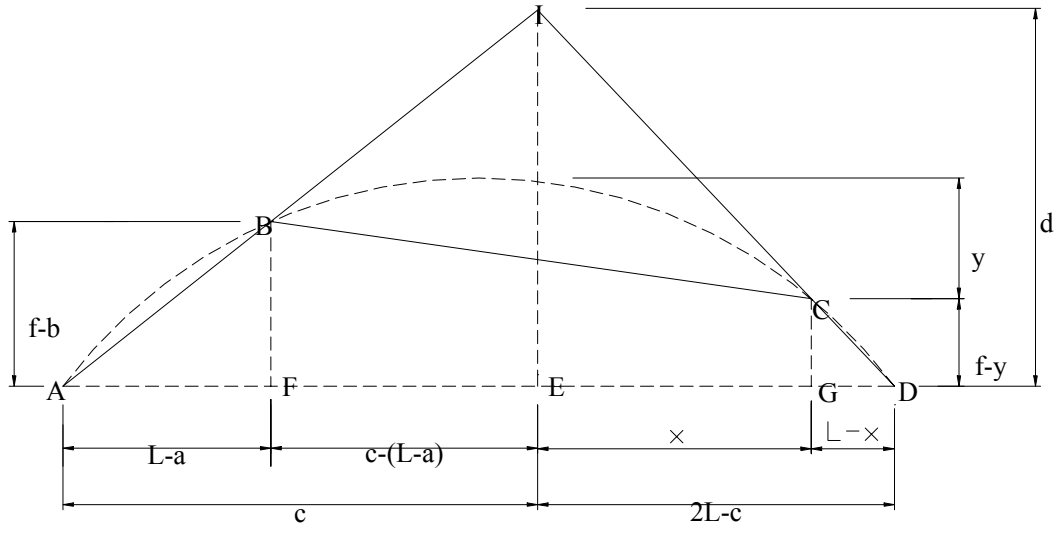

Figure 2.6 – Calculation of the elevation of the center of rotation I

Azurém, P – 4800-058 Guimarães Tel. +351 253 510200 • Fax +351 253 510217

The similarity of triangles ΔAIE and ΔABF yields

$$\frac{d}{c}=\frac{f-b}{L-a} \;\Rightarrow\; c=\frac{L-a}{f-b}\cdot d \tag{2.43}$$

and the similarity of triangles ΔDIE and ΔCDG yields

$$\frac{d}{2L-c}=\frac{f-y}{L-x} \;\Rightarrow\; d=\frac{f-y}{L-x}\cdot(2L-c). \tag{2.44}$$

Introducing Eq. (2.43) in Eq. (2.44), the value of the elevation *d* reads

$$d=\frac{2\cdot L}{\left(\frac{L-x}{f-y}+\frac{L-a}{f-b}\right)}. \tag{2.45}$$

Finally, using Eqs. (2.34) and (2.42), the equation of virtual work, Eq. (2.27), becomes,

$$P=\frac{Mp_1}{L-a}\left(1+\frac{f-b}{d-(f-b)}\right)+\frac{Mp_2}{L-a}\left(\frac{d-(f-y)}{(f-y)}\cdot\frac{(f-b)}{d-(f-b)}+\frac{f-b}{d-(f-b)}\right), \tag{2.38a}$$

which can be elaborated as

$$P=\frac{Mp_1}{L-a}\left(1+\frac{f-b}{d-(f-b)}\right)+\frac{Mp_2}{L-a}\left(\frac{(f-b)}{d-(f-b)}\cdot\frac{d}{(f-y)}\right). \tag{2.38b}$$

Introducing the value of *d*, from Eq. (2.37), and *a*, which is equal to *L*/2, and the parabolic shape, from which the values of *b* and *y* can be calculated, into Eq. (2.38b) and recasting this last equation, it is possible to obtain

$$P=48Mp_1\cdot\frac{L+x}{(9L+18x)\cdot L}+36Mp_2\cdot\frac{L}{(9L+18x)\cdot(L-x)}. \tag{2.38c}$$

Azurém, P – 4800-058 Guimarães Tel. +351 253 510200 • Fax +351 253 510217

Again the location of the second plastic hinge is given by the unknown distance x in Eq. (2.38c), which can be obtained by taking a derivative of P with respect to x and setting it equal to zero. Thus,

$$\frac{dP}{dx} = -\frac{48}{(3L+6x)^2}\cdot Mp_1 - \frac{12\mathrm{L}\cdot(3\mathrm{L}-12\mathrm{x})}{\left(3L^2+3Lx-6x^2\right)^2}\cdot Mp_2 = 0\,. \tag{2.39}$$

Solving this equation, it is possible to obtain

$$x = \frac{L}{8Mp_1}\cdot\left(8Mp_1+12Mp_2-12\sqrt{Mp_1Mp_2+(Mp_2)^2}\right). \tag{2.40}$$

Again, the values of x from Eq. (2.40), obtained for given values of Mp_1 and Mp_2, are shown in Table 2.3. Once the location of the second hinge is known, Eq. (2.38c) allows obtaining the value of the ultimate load P_u. The values obtained are equal to those obtained through the static approach, which should be expected from the uniqueness theorem of plastic analysis.

Table 2.3 – Values of the location x for the second plastic hinge and of the ultimate load P_u, for given values of Mp_1 and Mp_2

Mp_1	Mp_2	h_2	x	P_u
Mp	0	0	L	∞
Mp	Mp	$0.386f$	$0.379L$	$15.70Mp/L$
Mp	$0.5Mp$	$0.301f$	$0.451L$	$8.73Mp/L$

Azurém, P – 4800-058 Guimarães Tel. +351 253 510200 • Fax +351 253 510217

3 Application for ISOBRICK Shells

The purpose of the present work is to present design criteria for industrialized masonry vaults. In the preceding sections, design criteria were given, using both elastic and plastic analysis. The vault is two-pinned and carries a single concentrated load, at a quarter span, even if extension to other loading conditions is straightforward. Here, the obtained design criteria are used to determine the collapse loads for the vaults tested by Sarrablo (2002). The calculated values will be compared with the experimental collapse loads.

Table 3.1 presents the material and geometry properties, as well as the collapse loads of the five vaults P_u tested by Sarrablo (2002). Here ρ is the percentage of longitudinal reinforcement, f_y is the yield strength of the reinforcement (assumed equal to the Steel Class, as no tests have been carried out), $f_{c,\,cubes}$ is the compressive strength of the mortar measured in cubes, f_{cm} is the calculated actual compressive strength of the mortar and f_{tm} is the tensile strength of the mortar.

Table 3.1 – Material and geometry properties and collapse loads for the vaults

Vault	Reinforcement			Mortar				P_u
	No. of bars	ρ (%)	f_y (N/mm^2)	Strength (N/mm^2)	$f_{c,\,cubes}$ (N/mm^2)	f_{cm}^* (N/mm^2)	f_{tm} (N/mm^2)	(kN)
1 / 2	5 ϕ 8	0.31	500	Low	13.0 / 21.0	16.8	1.29*	21.0
3	5 ϕ 8	0.31	500	High	56.3	45.0	2.20**	26.0
4	5 ϕ 6	0.17	400	High	53.5	42.8	2.00	15.2
5	5 ϕ 6	0.17	400	Low	38.6	22.6	1.70	14.2

* Calculated ** Estimated

In Table 1.3, the calculated compressive strength of mortar f_{cm} is equal to 0.8 $f_{c,\,cubes}$, because the values from Sarrablo (2002) have been obtained in mortar cubic specimens according to EN 1015-11. In the case of vault 1 / 2, tests to determine the tensile strength of the mortar f_{tm} were not carried out. Therefore, the tensile strength has been estimated from $1.4\times\left[\left(f_{cm}-8\right)/10\right]^{2/3}$, CEB-FIP (1993). In the case of vault 3, Sarralbo (2002) indicates an extremely high value, and the adopted value in this case has been extrapolated from vault 4.

Azurém, P – 4800-058 Guimarães Tel. +351 253 510200 • Fax +351 253 510217

The dimensions of the cross section of the vaults, see Figure 3.1, and the geometry of test model, see Figure 3.2, are given in Table 3.2. Here, *d* is the effective height of the cross section, *b* is the width of the vault, *h* is the height of the cross section, *L* is the span of the vault, *q* is the self-weight of the vault and *f* is the rise of the vault.

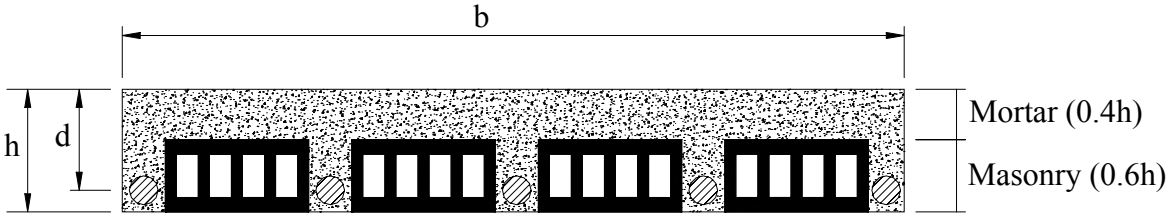

Figure 3.1 – Cross-section of the vaults

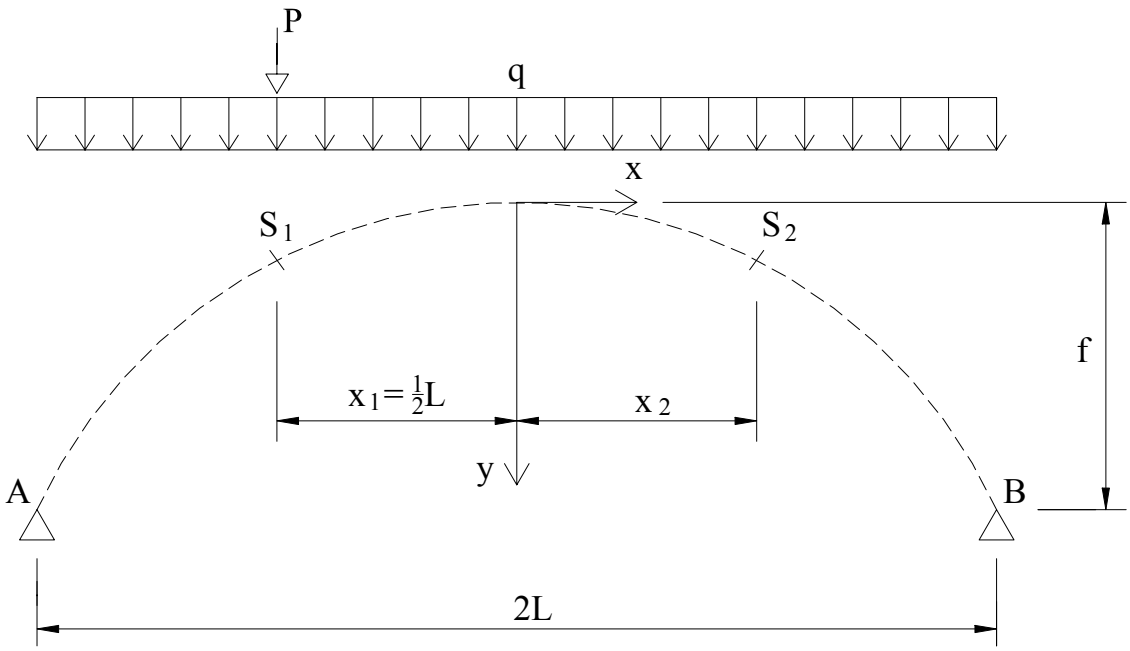

Figure 3.2 – View of the tested vault with its correspondent plastic hinge locations

Table 3.2 – Data for the tested vaults (see Figure 3.1 and Figure 3.2)

d (mm)	*b* (mm)	*h* (mm)	*L* (mm)	*q* (N/mm)	*f* (mm)
60	1090	75	4000	0.0015478	1000

With respect to the experimental values obtained for the distance x_2, which gives the location of formation of the second plastic hinge, Sarrablo (2002) only says that this location, for all the tested vaults, is in a region symmetrical to the position of the application of load *P*.

Azurém, P – 4800-058 Guimarães Tel. +351 253 510200 • Fax +351 253 510217

3.1 Elastic Design Results

Table 3.3 shows the numerical results calculated assuming elastic behavior for the vaults. Linear elastic analysis, based on the theory of elasticity, has been widely used for the verification of both ULS and SLS of e.g. reinforced concrete structures. But, for serviceability limit states, a gradual evolution of cracking should be considered and, for ultimate limit states, careful detailing of the reinforcement to cover all zones where tensile stresses may appear is required. As there is no upper (extrados) reinforcement in the vault, the elastic analysis can only be used up to cracking of the upper layer of the vault.

This is shown in Table 3.3, which presents the results of the internal forces N and M at sections S_1 (left plastic hinge) and S_2 (right plastic hinge) and the corresponding stresses (see Figure 3.2). These results were obtained by using eqs. (2.10), (2.11), and (2.1), respectively. Here P^e_{ult} indicates the point load, once the maximum tensile strength of the upper layer of the vault is reached. The maximum tensile strength is reached at a position x_2, which indicates the most likely location of the right "plastic" hinge. Table 3.4 indicates also that the maximum tensile stresses occur in the cross-section under the load application, here, denoted as left plastic hinge. As this region includes bottom reinforcement, the critical section is the right plastic hinge.

Table 3.3 – Numerical results for elastic analysis: (a) internal forces and (b) tensile stresses

(a)

Vault	P^e_u (kN)	Plastic hinge one		Plastic hinge two	
		N_1 (kN)	M_1 (kN.m)	N_2 (kN)	M_2 (kN.m)
1 / 2	6.68	-9.26	2.03	-7.66	-1.34
3	11.65	-13.57	3.54	-10.86	-2.33
4	10.75	-12.79	3.27	-10.27	-2.15
5	9.13	-11.38	2.78	-9.23	-1.82

(b)

Vault	Plastic hinge one		Plastic hinge two	
	x_1 (mm)	σ_{bot} (N/mm^2)	x_2 (mm)	σ_{top} (N/mm^2)
1 / 2	-1000	2.03	828	1.29
3	-1000	3.44	816	2.20
4	-1000	3.13	800	2.00
5	-1000	2.67	812	1.70

Azurém, P – 4800-058 Guimarães Tel. +351 253 510200 • Fax +351 253 510217

For vault 1 / 2, the detailed results of the internal forces (axial force and bending moment) and maximum normal stresses over the span of the arch are given in Table 3.4, where the bold figures indicate the location of the plastic hinges. The diagram of the axial force, see Figure 3.3, indicates that the axial force exhibits moderate variation to the left and right sides of the point load, with a severe jump at this location. The diagram of the bending moment indicates clearly a maximum positive bending moment under the point load and a maximum negative bending moment at the location of the second hinge. The ratio between the maximum bending moments (positive and negative) is 1.5.

Annex A provides similar results for the other vaults tested by Sarralbo (2002), namely vaults 3, 4 and 5.

Table 3.4 – Forces and stresses over the span of vault 1 / 2

Geometry - middle line			Internal forces		Stresses	
X (mm)	y (mm)	$\theta = arctan(y')$ (degree)	$N(\theta)$ (kN)	$Ms(x,y)$ (kN.m)	σ_{top} (N/mm^2)	σ_{bot} (N/mm^2)
-2000	0	45.00	-10.74	0	-0.13	-0.13
-1800	190	41.99	-10.48	0.25	-0.38	0.13
-1600	360	38.66	-10.20	0.57	-0.72	0.47
-1400	510	34.99	-9.91	0.98	-1.14	0.89
-1200	640	30.96	-9.60	1.47	-1.64	1.40
-1000	**750**	**26.57**	**-9.26**	**2.03**	**-2.22**	**1.99**
-1000	**750**	**26.57**	**-6.27**	**2.03**	**-2.18**	**2.03**
-800	840	21.80	-6.41	1.34	-1.47	1.31
-600	910	16.70	-6.56	0.73	-0.83	0.67
-400	960	11.31	-6.73	0.19	-0.28	0.12
-200	990	5.71	-6.90	-0.26	0.18	-0.35
0	1000	0.00	-7.07	-0.63	0.57	-0.74
200	990	-5.71	-7.23	-0.93	0.87	-1.05
400	960	-11.31	-7.38	-1.14	1.09	-1.27
600	910	-16.70	-7.52	-1.28	1.23	-1.42
828	**829**	**-22.49**	**-7.66**	**-1.34**	**1.29**	**-1.48**
1000	750	-26.57	-7.77	-1.31	1.26	-1.45
1200	640	-30.96	-7.88	-1.21	1.15	-1.35
1400	510	-34.99	-8.00	-1.02	0.96	-1.16
1600	360	-38.66	-8.11	-0.76	0.69	-0.89
1800	190	-41.99	-8.24	-0.42	0.34	-0.54
2000	0	-45.00	-8.37	0	-0.10	-0.10

Azurém, P – 4800-058 Guimarães Tel. +351 253 510200 • Fax +351 253 510217

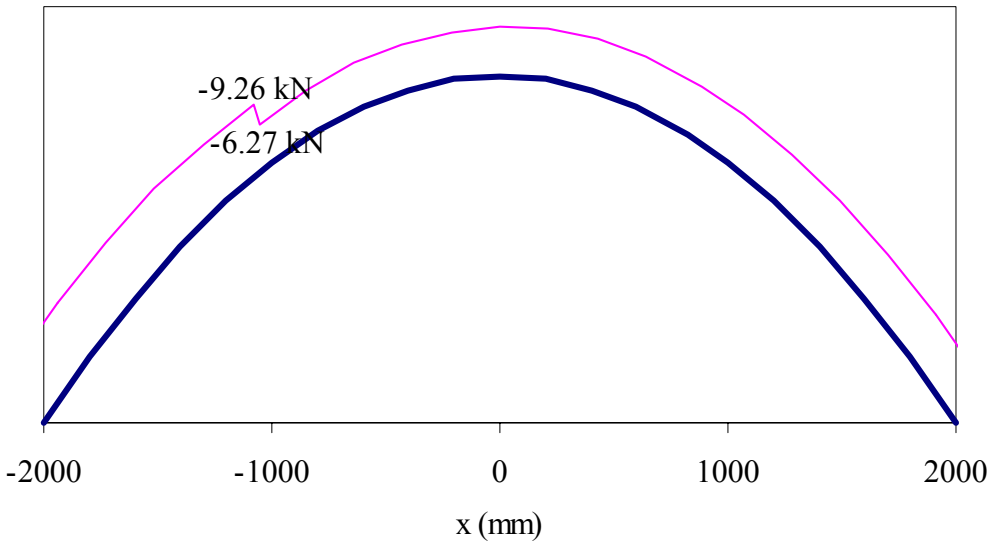

Figure 3.3 – Axial diagram force for vault 1 / 2

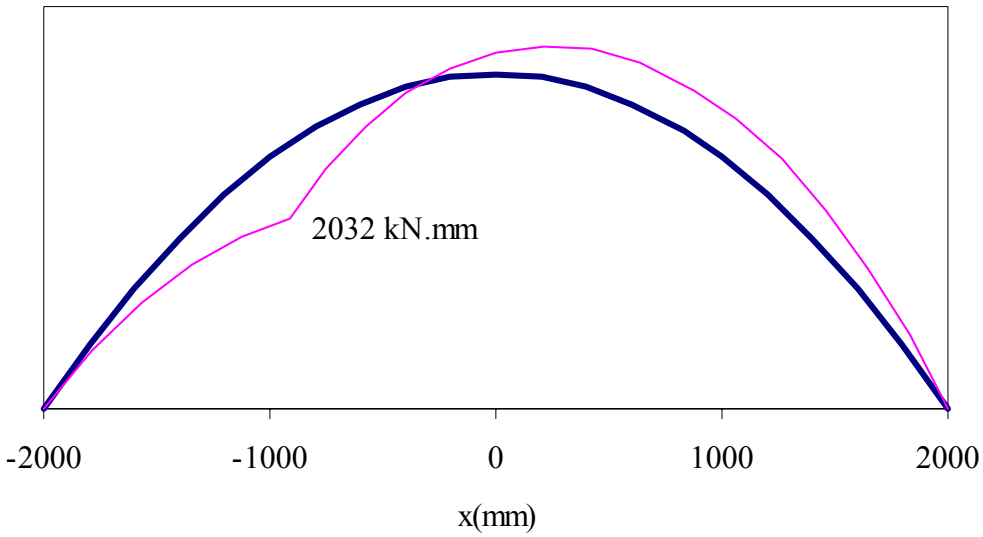

Figure 3.4 – Bending moment diagram for vault 1 / 2

Finally, Table 3.5 presents a summary of the internal forces (axial force and bending moment) at the left hinge, for the maximum load $P_u = P^e_u$. The cracking load P^e_u is also compared with the ultimate experimental load. It can be seen that, as it is normal in concrete structures, cracking occurs before collapse (between 30% and 70% of the maximum load). After cracking significant load redistributions occur, as mortar possesses a quasi-brittle behavior. In addition, the amount of bottom reinforcement necessary at the cracking stage, and the existing reinforcement are compared. It can be seen that the ratio between loads is rather different from the ratio between reinforcements, meaning that elastic design cannot be

Azurém, P – 4800-058 Guimarães Tel. +351 253 510200 • Fax +351 253 510217

used unless top and bottom reinforcement are considered, which has not been the case in the present testing program. However, for the present testing program, elastic analysis seems of interest as a tool to define the position of the second (right) hinge.

Table 3.5 – Numerical results for elastic analysis at left hinge

Vault	P_u Testing (kN)	P^e_u (kN)	$\frac{P^e_u}{P_u}$	Internal Forces		Adequacy of design		
				N (kN)	M (kN.m)	$A_{s,\,required}$ (mm^2)	$A_{s,\,existent}$ (mm^2)	$\frac{A_{s,\,req}}{A_{s,\,exist}}$
1 / 2	21.0	6.68	0.32	-9.26	2.03	57	251	0.23
3	26.0	11.65	0.45	-13.57	3.54	103	251	0.41
4	15.2	10.75	0.71	-12.79	3.27	118	141	0.84
5	14.2	9.13	0.64	-11.38	2.78	100	141	0.71

3.2 Plastic Design Results

Design of the masonry vaults, reinforced only at the bottom (intrados), is better carried out using plastic analysis. According to the formulas of plastic design presented to determinate the collapse load P_u, Eq. (2.38c) and Eq. (2.40), it is necessary to know the values of the plastic moments at the left and right hinges, respectively Mp_1 and Mp_2. However, since the cross section of the arch is subjected to combined bending and compression, it is necessary to consider the interaction of the bending moment M and the normal force N. This N-M interaction diagram can then be used for taking into account the internal forces acting in the cross-section. Thus, the N-M interaction diagram for each vault was constructed and the reader is referred to Annex B for this information.

Given the fact that the axial loading depends on the point load P_u at ultimate stage, an iterative process is proposed here, according to the following steps:

a) The axial forces N_1 and N_2, acting in the sections of left and right plastic hinges, are calculated by using the elastic analysis detailed in Section 3.1. The iterative process is started (iteration i = 0) with an initial load $P_i=P^e_u$ and an initial location of the right plastic hinge $x_i=x^e$, which are the values obtained in the elastic analysis. As discussed before, the distance x defines the location of plastic hinge two and P is the point load applied at ¼ span of the vault.
b) $(Mp_1)_i$ is obtained in the N-M interaction diagram by linear interpolation and $(Mp_2)_i$ is obtained by the following equation,

Azurém, P – 4800-058 Guimarães Tel. +351 253 510200 • Fax +351 253 510217

$$\left(Mp_2\right)_i = Mcr = \left[f_{tm} - \frac{\left(N_2\right)_i}{A_o} \right] \cdot \frac{I_o}{c_{top}} . \tag{3.2}$$

c) The values of P_i and x_i are calculated using Eq. (2.38c) and Eq. (2.40), respectively;

d) Calculate the ratio R, used as a stop criterion for the iterative process,

$$R_i = \left(1 - \frac{P_{i-1}}{P_i} \right) \cdot 100 ; \tag{3.3}$$

e) The iteration process is stopped once $R_i \leq 1\%$. If $R_i \geq 1\%$, then a new iteration $i + 1$ will be carried out, for which a new elastic analysis will be performed using $P_{i+1} = P_i$. It is noted that the self-weight of the vault is being taken into account at this stage.

As it is possible to observe at step b), different procedures have been used to calculate the plastic moments Mp_1 and Mp_2. For the section of plastic hinge one, the usual ultimate bending moment Mp_1 was used, with mortar under compression and reinforcement (intrados) under tension. Therefore, its strength capacity is given by *N-M* interaction diagram of Annex B. For the section of plastic hinge two, no reinforcement is present and the adopted value, at this stage, Mp_2 is equal to the cracking moment *Mcr*. This is a questionable option as the behavior of mortar in tension is quasi-brittle and for design purposes should be considered equal to zero.

Figure 3.5 details the steps of the iterative process described above to evaluate the ultimate load P_u.

Azurém, P – 4800-058 Guimarães Tel. +351 253 510200 • Fax +351 253 510217

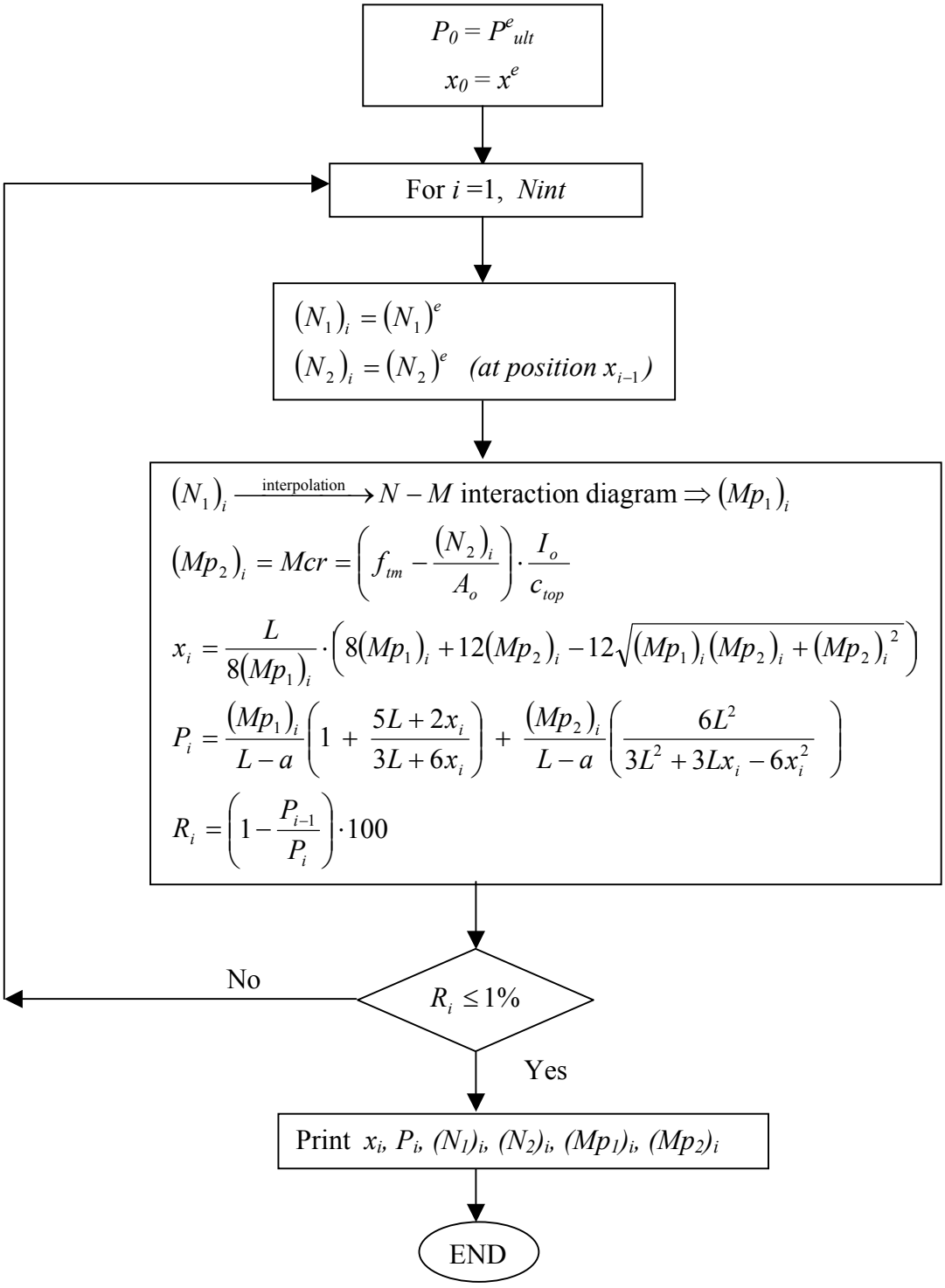

Figure 3.5 – Iterative process to calculate the ultimate load P_u.

Tables 3.5 to 3.8 show the values obtained for the different vault, using the iterative process.

Azurém, P – 4800-058 Guimarães Tel. +351 253 510200 • Fax +351 253 510217

Table 3.5 – Plastic design results for vault 1/2

Iter	x_2 (mm)	P^p_u (kN)	N_1 (kN)	N_2 (kN)	Mp_1 (kN.m)	Mp_2 (kN.m)	R (%)
1	828	6.68	-9.26	-7.66	7.31	1.34	100.00
2	1153	17.20	-18.39	-14.59	7.58	1.42	76.63
3	1147	17.91	-19.00	-15.04	7.60	1.42	3.93
4	1147	17.96	-19.04	-15.07	7.60	1.42	0.26

Table 3.6 – Plastic design results for vault 3

Iter	x_2 (mm)	P^p_u (kN)	N_1 (kN)	N_2 (kN)	Mp_1 (kN.m)	Mp_2 (kN.m)	R (%)
1	816	11.65	-13.57	-10.86	7.82	2.33	100.00
2	1028	20.30	-21.07	-16.24	8.08	2.34	42.58
3	1029	20.95	-21.64	-16.96	8.10	2.40	3.12
4	1029	21.00	-21.68	-17.00	8.10	2.40	0.25

Table 3.7 – Plastic design results for vault 4

Iter	x_2 (mm)	P^p_u (kN)	N_1 (kN)	N_2 (kN)	Mp_1 (kN.m)	Mp_2 (kN.m)	R (%)
1	800	10.76	-12.79	-10.27	3.82	2.15	100.00
2	875	11.87	-13.76	-11.04	3.85	2.16	9.41
3	876	11.96	-13.84	-11.10	3.85	2.16	0.74
4	876	11.97	-13.85	-11.10	3.85	2.16	0.06

Table 3.8 – Plastic design results for vault 5

Iter	x_2 (mm)	P^p_u (kN)	N_1 (kN)	N_2 (kN)	Mp_1 (kN.m)	Mp_2 (kN.m)	R (%)
1	812	9.13	-11.38	-9.23	3.74	1.82	100.00
2	908	11.11	-13.10	-10.57	3.80	1.84	17.80
3	909	11.26	-13.23	-10.67	3.81	1.84	1.37
4	910	11.27	-13.24	-10.67	3.81	1.84	0.11

The convergence of the iterative process is rather fast, with convergence after four interactions. For the purpose of validation of easiness of comparison, Table 3.9 presents a summary of the results obtained in the plastic analysis for the maximum plastic load P^p_u. The values of P^p_u are then compared in Table 3.10 with those were obtained experimentally, and also with the results of elastic analysis.

Azurém, P – 4800-058 Guimarães Tel. +351 253 510200 • Fax +351 253 510217

Table 3.9 – Numerical results for plastic analysis

Vault	$P^p{}_u$	Plastic hinge one			Plastic hinge two		
	(kN)	x_1 (mm)	N_1 (kN)	M_1 (kN.m)	x_2 (mm)	N_2 (kN)	M_2 (kN.m)
1 / 2	17.96	-1000	-19.04	7.60	1147	-15.07	1.42
3	21.00	-1000	-21.68	8.10	1029	-17.00	2.40
4	11.97	-1000	-13.85	3.85	876	-11.10	2.16
5	11.27	-1000	-13.24	3.81	910	-10.67	1.84

Table 3.10 – Comparisons between calculated and testing P_u

Vault	P_u	Elastic analysis			Plastic analysis		
	Testing (kN)	x_2 (mm)	$P^e{}_u$ (kN)	$\frac{P^e_u}{P_u}$	x_2 (mm)	$P^p{}_u$ (kN)	$\frac{P^p_u}{P_u}$
1 / 2	21.0	828	6.68	0.32	1147	17.9	0.86
3	26.0	816	11.65	0.45	1029	21.0	0.81
4	15.2	800	10.75	0.71	876	11.9	0.79
5	14.2	812	9.13	0.64	910	11.2	0.79

Clearly, in terms of ultimate load, the results from plastic analysis are much better than those of elastic analysis. Nevertheless, the plastic analysis results still lay around 15% to 20% below the experimental load, even if the cracking moment at the right hinge M_{p2} is assumed as fully plastic. It is believed that the main reason for the differences found are due to the lack of information on the constitutive behavior of the adopted steel. It is noted that the relation between the calculated ultimate load and the observed failure load does not vary significantly, with no variation for vaults 4 and 5 (steel S400, same series and same rebars) and around 6% variation for vaults 1 / 2 and 3 (steel S500, different series).

Another interesting point is that the process adopted allows for (moderate) variation of the location of the plastic hinge x_2. This procedure is also questionable because, once the crack occurs in the top surface, the location of the "hinge" is fixed.

It is also of relevance to discuss the differences in ultimate load, between vaults 1 / 2 and 3, hereby denoted as Group I, and vaults 4 / 5, hereby denoted as Group II. These groups of vaults exhibit the same percentage of longitudinal reinforcement (ρ) but different mortar strength. For Group I, in which ρ is almost twice larger than Group II, mortar strength plays an important role in the ultimate strength of the vault, as can be seen in the experimental load-displacement diagram (Figure 3.5a). The influence of the mortar strength indicates that failure is accompanied by mortar crushing at the left hinge. For Group II, with a lower ρ, the mortar

Azurém, P – 4800-058 Guimarães Tel. +351 253 510200 • Fax +351 253 510217

strength does not influence the failure load of the vault (see Figure 3.5b), as solely yielding of the reinforcement controls collapse. This is very well reproduced by the plastic analysis.

Additionally, the ratio between the bottom reinforcement for Group I and Group II (251 / 141 = 1.78) is similar to the ratio between the calculated collapse loads with plastic analysis (21.0 / 11.9 =1.76). Here, the maximum values of the mortar strength are used, in order to override the influence of mortar crushing. Again, this similitude stresses the adequacy of plastic analysis.

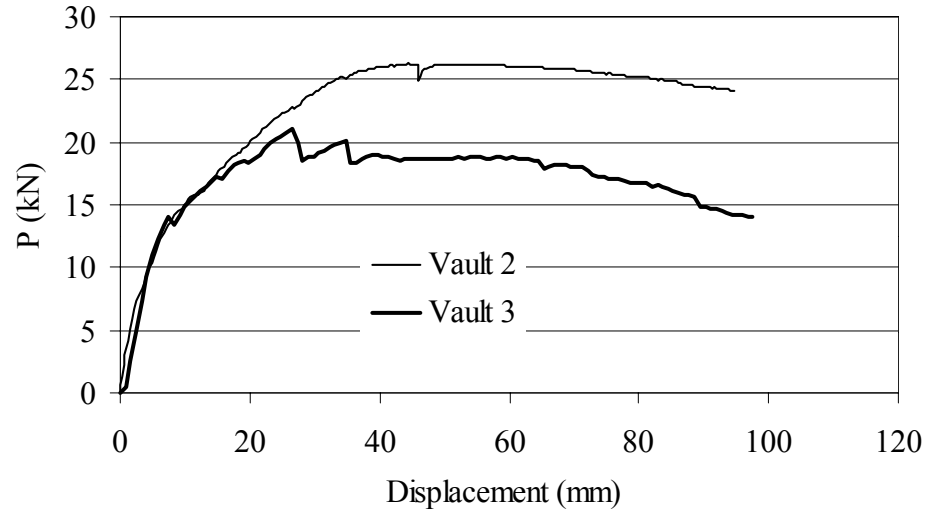

(a)

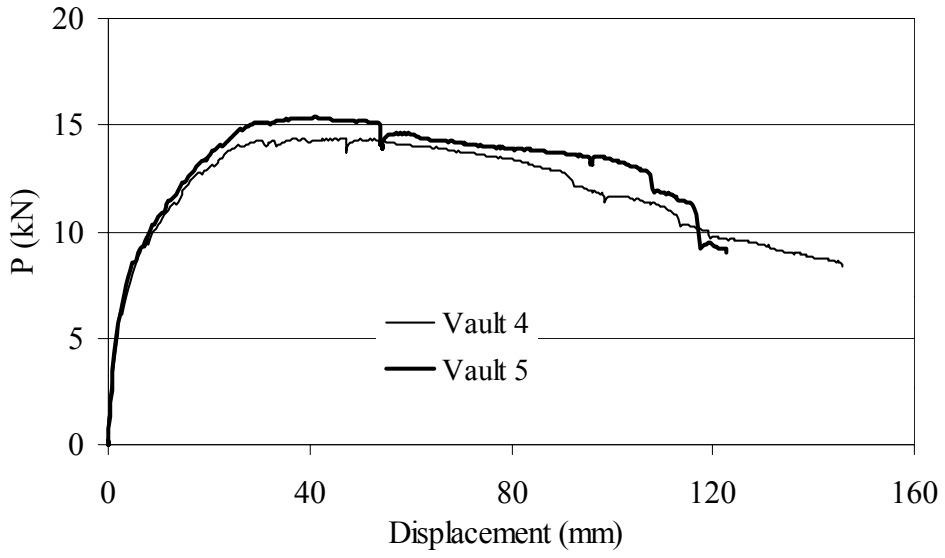

(b)

Figure 3.5 – Experimental load-displacement diagrams for the vaults, in groups of equal reinforcement, Sarrablo (2002): (a) Group I – vaults 2 and 3; (b) Group II – vaults 4 and 5.

Azurém, P – 4800-058 Guimarães Tel. +351 253 510200 • Fax +351 253 510217

4 Recommendations for Design

In the previous Section, the tensile strength was considered for the sake of assessment of plastic analysis. This hypothesis is questionable from the theoretical point of view but also from a practical point of view, as it constitutes a violation with respect to codes. In fact, the tensile strength of cement-based materials should be considered equal to zero for the verification of the ultimate limit states. Therefore, a new set of analyses has been carried out, assuming $f_{tm} = 0$. The results were obtained by applying the iterative process described before and the complete results can be found in Annex C.

Table 4.1 gives the results of this new analysis. Here, $P_u^{p,ref}$ represents the reference value for ultimate load calculated in the previous section, using plastic analysis. It can be seen that very significant differences are found both in terms of ultimate loads (060-0.80 of the reference value) and also of the location of the right hinge. Due to the low value of M_{p2}, the hinge is very close to the right support. This is not confirmed by experimental testing, being therefore not recommended for practical application.

Table 4.1 – Plastic analysis results for $f_{tm} = 0$

Vault	$P^p{}_u$	Plastic hinge one			Plastic hinge two			$\frac{P_u^p}{P_u^{p,ref}}$
	(kN)	x_1 (mm)	N_1 (kN)	M_1 (kN.m)	x_2 (mm)	N_2 (kN)	M_2 (kN.m)	
1 / 2	14.44	-1000	-15.99	7.51	1629	-12.94	0.15	0.80
3	15.26	-1000	-16.70	7.93	1626	-13.44	0.16	0.73
4	7.24	-1000	-9.74	3.70	1574	-8.44	0.10	0.60
5	7.20	-1000	-9.70	3.68	1574	-8.42	0.10	0.64

In order to eliminate the drawback of the previous approach to solve engineering applications, one possibility is to use the location of the right hinge according to the elastic analysis. In the absence of upper reinforcement, this is the most likely location of the right hinge. If this is the case, it is possible to adopt $M_{p2} = 0$, as the collapse mechanism is perfectly defined. In such a case, Eq. (2.38c) is directly applicable as the location of the right hinge x (or x_2) is no longer resulting from a minimization process, see again Annex C.

Table 4.2 gives the results of this second new analysis. Again, it can be seen that very significant differences are found, but only in terms of ultimate loads (065-0.85 of the reference value), as the location of the right hinge is predefined. This conservative ultimate load seems adequate for practical applications at this stage. The new experiments being

Azurém, P – 4800-058 Guimarães Tel. +351 253 510200 • Fax +351 253 510217

carried out in the framework of the ISOBRICK project, with convenient characterization of the reinforcement steel, together with the advanced simulations with finite elements will allow a final conclusion regarding this matter.

Table 4.2 – Plastic analysis results for $Mp_2 = 0$ and fixed x_2

Vault	$P^p{}_u$	Plastic hinge one			Plastic hinge two			$\frac{P_u^p}{P_u^{p,ref}}$
	(kN)	x_1 (mm)	N_1 (kN)	M_1 (kN.m)	x_2 (mm)	N_2 (kN)	M_2 (kN.m)	
1 / 2	15.54	-1000	-16.95	7.54	828	-13.38	0.0	0.86
3	16.47	-1000	-17.75	7.96	816	-13.97	0.0	0.78
4	7.72	-1000	-10.15	3.72	800	-8.31	0.0	0.64
5	7.65	-1000	-10.10	3.70	812	-8.28	0.0	0.68

Finally, Figure 4.1 shows the *N-M* interaction diagram for vault 1 / 2, at ultimate load calculated with plastic analysis. The graph shows that, for the loads, arch shape and thickness considered, the influence of the axial force is minor for the calculation of the plastic moment at the left hinge. As shown above, i.e. values of M_2 in Table 4.1, the influence of the axial force is again minor, for the calculation of the right hinge cracking moment. Therefore, for practical purposes, the axial force can be ignored. This procedure simplifies the analysis to great extent (no need to consider any iterative procedure).

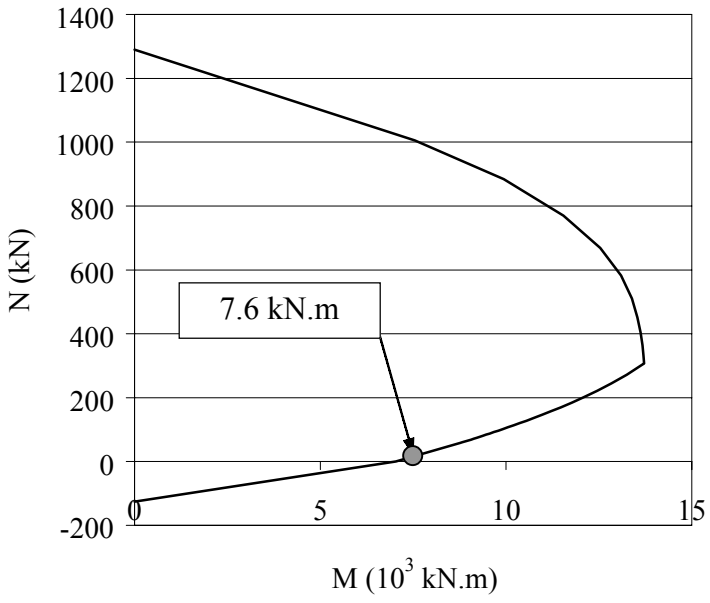

Figure 4.1 – *N-M* interaction diagram for vault 1 / 2, with location of the position of the left plastic hinge, at ultimate load calculated with plastic analysis

Azurém, P – 4800-058 Guimarães Tel. +351 253 510200 • Fax +351 253 510217

5 Conclusions

This report provides a comprehensive study on design criteria for industrialized masonry vaults, using both elastic and plastic analysis formulations. The formulations were compared with a series of vaults tested by Sarrablo (2002). The lack of experimental information on the reinforcement steel hinders moderately the conclusions of this study.

Nevertheless, it is possible to establish the following conclusions:

- Elastic analysis is inadequate to analyze arches, unless upper and lower reinforcement are provided. In the case of placing both upper and lower reinforcement, the usage of elastic analysis does not allow load redistributions;
- An iterative procedure to calculate the ultimate load of an arch, using plastic analysis, has been presented. The numerical results are in good agreement with experimental results;
- In an arch loaded with a point load at the left quarter span and without upper reinforcement, the location of the right hinge is controlled by the tensile strength of the top screed. This parameter influences the ultimate load significantly. Therefore, it is recommended to provides always a minimum amount of upper reinforcement;
- For the case of the ISOBRICK vaults with a point load at quarter span and catenary shape, the self-weight of the arch has marginal effect on the analysis and can be ignored for practical purposes. In this case, if upper reinforcement is not provided (or is below the minimum requirement), it is recommended to define the location of the right hinge x using linear elastic analysis. Then, the ultimate load is given by

$$P = 48Mp_1 \cdot \frac{L + x}{(9L + 18x) \cdot L},$$

where L is half the span of the arch and M_{p1} is the ultimate bending moment associated with the lower reinforcement.

If upper reinforcement is provided, the location of the right hinge x and the ultimate load P are given by

$$x = \frac{L}{8Mp_1} \cdot \left(8Mp_1 + 12Mp_2 - 12\sqrt{Mp_1 Mp_2 + (Mp_2)^2} \right)$$

Azurém, P – 4800-058 Guimarães Tel. +351 253 510200 • Fax +351 253 510217

$$P = 48Mp_1 \cdot \frac{L+x}{(9L+18x)\cdot L} + 36Mp_2 \cdot \frac{L}{(9L+18x)\cdot(L-x)}$$

where L is half the span of the arch, M_{p1} is the ultimate bending moment associated with the lower reinforcement and M_{p2} is the ultimate bending moment associated with the upper reinforcement.

Azurém, P – 4800-058 Guimarães Tel. +351 253 510200 • Fax +351 253 510217

6 References

CEB (1993) - CEB-FIP Model Code 1990, Bulletin d'Information nº 213/214, Thomas Telford, London, UK.

GIURIANI, E.; GUBANA, A.; ARENGHI, A. (2001) - Structural rehabilitation of masonry vaults, In: UNESCO-ICOMOS Millennium Congress, Paris, France, 10-12 Sept., Proceedings.

RODRIGUEZ, F. and AZCUNAGA, A. (1980) – Strength of materials (in Spanish), Escuela Tecnica Superior de Ingenieros Industriales, Madrid, Spain, p. 51-71.

SARRALBO, V. (2002) - Contribution to the viability of laminar reinforced masonry roofs using semi-prefabricated solutions. Proposal for short span cylindrical shells (in Spanish), PhD Thesis, Universitat Politècnica de Catalunya, Barcelona, Spain.

Azurém, P – 4800-058 Guimarães Tel. +351 253 510200 • Fax +351 253 510217

ANNEX A

Elastic Results for Vault s for Vault Series 3, 4 and 5

Table A.1 – Forces and stresses over the span of vault 3

Geometry - middle line			Internal forces		Stresses	
x(mm)	y(mm)	θ=arctan(y')	N(θ) (kN)	Ms(x,y) (kN.m)	σ_{top} (N/mm^2)	σ_{bot} (N/mm^2)
-2000	0	45.00	-15.46	0	-0.19	-0.19
-1800	190	41.99	-15.17	0.43	-0.62	0.25
-1600	360	38.66	-14.84	1.00	-1.18	0.82
-1400	510	34.99	-14.47	1.71	-1.89	1.53
-1200	640	30.96	-14.05	2.5.6	-2.73	2.39
-1000	**750**	**26.57**	**-13.57**	**3.54**	**-3.71**	**3.38**
-1000	**750**	**26.57**	**-8.36**	**3.54**	**-3.65**	**3.44**
-800	840	21.80	-8.69	2.33	-2.44	2.23
-600	910	16.70	-9.04	1.27	-1.38	1.16
-400	960	11.31	-9.38	0.34	-0.45	0.22
-200	990	5.71	-9.72	-0.46	0.34	-0.57
0	1000	0.00	-10.03	-1.11	0.99	-1.23
200	990	-5.71	-10.30	-1.62	1.50	-1.75
400	960	-11.31	-10.53	-2.00	1.87	-2.13
600	910	-16.70	-10.71	-2.23	2.10	-2.36
816	**834**	**-22.20**	**-10.86**	**-2.33**	**2.20**	**-2.47**
1000	750	-26.57	-10.97	-2.29	2.16	-2.42
1200	640	-30.96	-11.06	-2.11	1.97	-2.24
1400	510	-34.99	-11.13	-1.79	1.65	-1.93
1600	360	-38.66	-11.20	-1.33	1.20	-1.47
1800	190	-41.99	-11.27	-0.74	0.60	-0.87
2000	0	-45.00	-11.34	0	-0.14	-0.14

The bold rows in Table A.1 show the values for left and right plastic hinges.

Azurém, P – 4800-058 Guimarães Tel. +351 253 510200 • Fax +351 253 510217

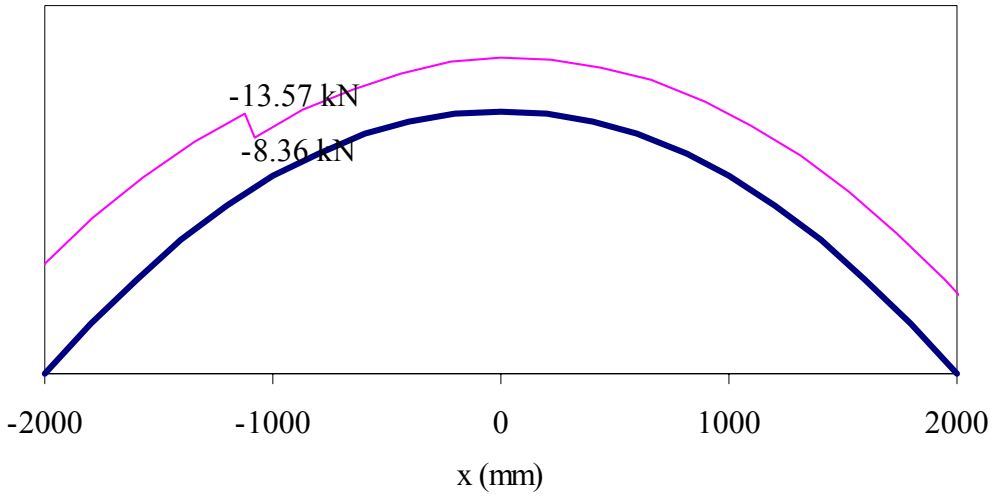

Figure A.1 – Axial force diagram for vault 3

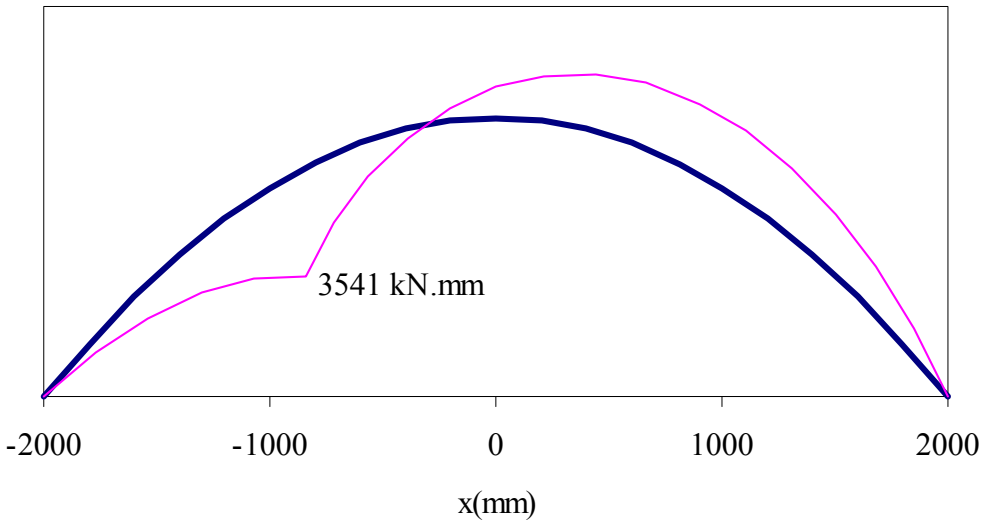

Figure A.2 – Bending moment diagram for vault 3

Azurém, P – 4800-058 Guimarães
Tel. +351 253 510200 • Fax +351 253 510217

Table A.2 – Forces and stresses over the span of vault 4

Geometry - middle line			Internal forces		Stresses	
x(mm)	y(mm)	θ=arctan(y')	N(θ) (kN)	Ms(x,y) (kN.m)	σ_{top} (N/mm^2)	σ_{bot} (N/mm^2)
-2000	0	45.00	-14.61	0	-0.18	-0.18
-1800	190	41.99	-14.32	0.4	-0.57	0.22
-1600	360	38.66	-14.00	0.92	-1.08	0.74
-1400	510	34.99	-13.65	1.58	-1.73	1.39
-1200	640	30.96	-13.25	2.36	-2.49	2.17
-1000	**750**	**26.57**	**-12.79**	**3.27**	**-3.39**	**3.08**
-1000	**750**	**26.57**	**-7.98**	**3.27**	**-3.33**	**3.13**
-800	840	21.80	-8.28	2.15	-2.23	2.03
-600	910	16.70	-8.59	1.17	-1.26	1.05
-400	960	11.31	-8.90	0.31	-0.42	0.20
-200	990	5.71	-9.21	-0.42	0.30	-0.53
0	1000	0.00	-9.50	-1.02	0.89	-1.13
200	990	-5.71	-9.75	-1.50	1.36	-1.60
400	960	-11.31	-9.96	-1.84	1.70	-1.94
600	910	-16.70	-10.13	-2.06	1.91	-2.16
800	**840**	**-21.80**	**-10.27**	**-2.15**	**2.00**	**-2.25**
1000	750	-26.57	-10.39	-2.11	1.96	-2.21
1200	640	-30.96	-10.48	-1.94	1.79	-2.05
1400	510	-34.99	-10.56	-1.65	1.50	-1.76
1600	360	-38.66	-10.64	-1.23	1.08	-1.34
1800	190	-41.99	-10.72	-0.68	0.54	-0.80
2000	0	-45.00	-10.80	0	-0.13	-0.13

The bold rows in Table A.2 show the values for left and right plastic hinges.

Azurém, P – 4800-058 Guimarães Tel. +351 253 510200 • Fax +351 253 510217

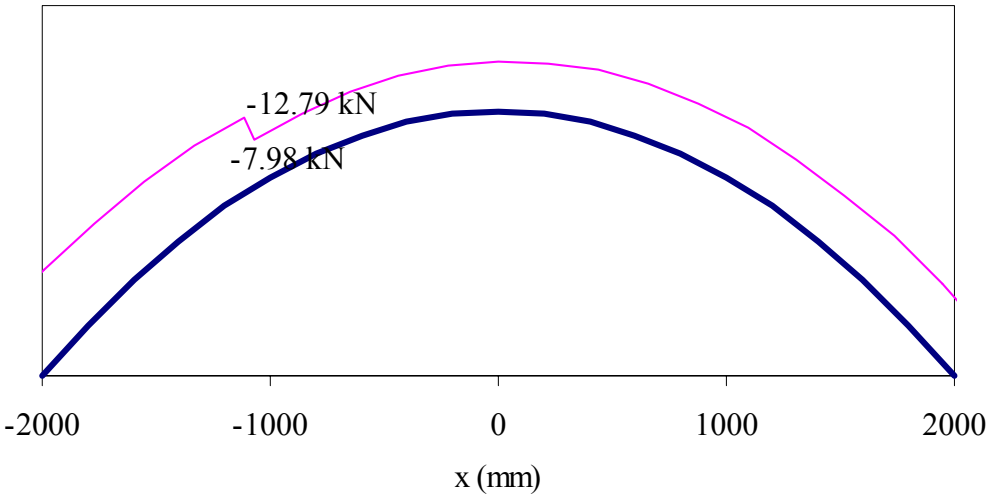

Figure A.3 – Axial force diagram for vault 4

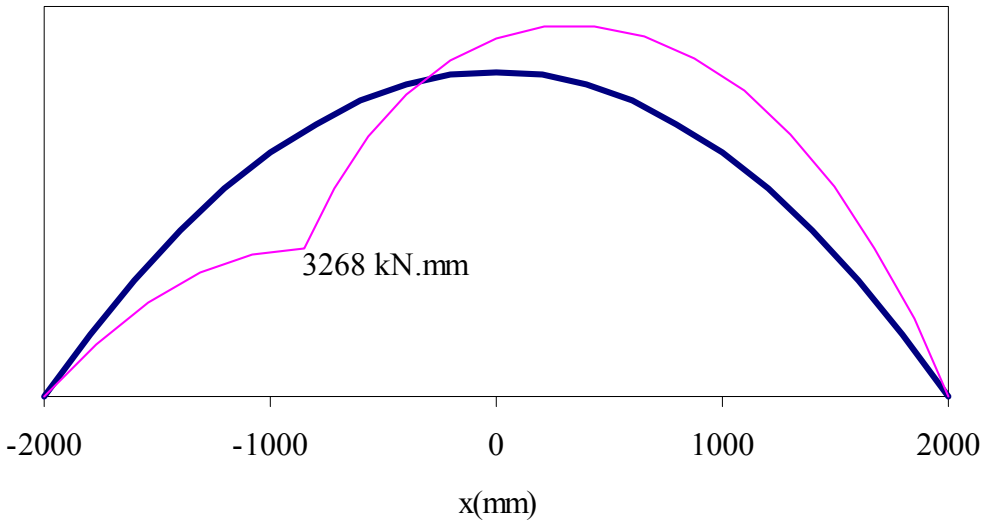

Figure A.4 – Bending moment diagram for vault 4

Azurém, P – 4800-058 Guimarães
Tel. +351 253 510200 • Fax +351 253 510217

Table A.3 – Forces and stresses over the span of vault 5

Geometry - middle line			Internal forces		Stresses	
x(mm)	y(mm)	θ=arctan(y')	N(θ) (kN)	Ms(x,y) (kN.m)	σ_{top} (N/mm^2)	σ_{bot} (N/mm^2)
-2000	0	45.00	-13.06	0	-0.16	-0.16
-1800	190	41.99	-12.78	0.34	-0.49	0.18
-1600	360	38.66	-12.48	0.78	-0.93	0.63
-1400	510	34.99	-12.16	1.34	-1.48	1.18
-1200	640	30.96	-11.79	2.00	-2.13	1.85
-1000	**750**	**26.57**	**-11.38**	**2.78**	**-2.90**	**2.62**
-1000	**750**	**26.57**	**-7.30**	**2.78**	**-2.85**	**2.67**
-800	840	21.80	-7.53	1.83	-1.91	1.73
-600	910	16.70	-7.78	0.99	-1.08	0.89
-400	960	11.31	-8.04	0.26	-0.36	0.16
-200	990	5.71	-8.29	-0.36	0.25	-0.45
0	1000	0.00	-8.53	-0.87	0.76	-0.97
200	990	-5.71	-8.74	-1.27	1.15	-1.37
400	960	-11.31	-8.93	-1.56	1.44	-1.66
600	910	-16.70	-9.09	-1.75	1.63	-1.85
812	**835**	**-22.10**	**-9.23**	**-1.82**	**1.70**	**-1.93**
1000	750	-26.57	-9.34	-1.79	1.67	-1.89
1200	640	-30.96	-9.44	-1.65	1.52	-1.76
1400	510	-34.99	-9.54	-1.40	1.28	-1.51
1600	360	-38.66	-9.63	-1.04	0.92	-1.15
1800	190	-41.99	-9.73	-0.58	0.45	-0.69
2000	0	-45.00	-9.83	0	-0.12	-0.12

The bold rows in Table A.3 show the values for left and right plastic hinges.

Azurém, P – 4800-058 Guimarães Tel. +351 253 510200 • Fax +351 253 510217

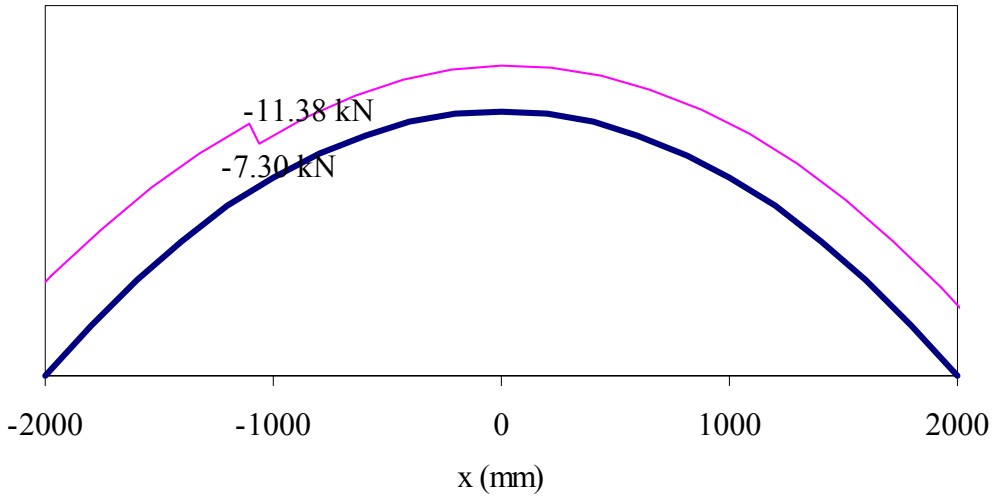

Figure A.5 – Axial force diagram for vault 4

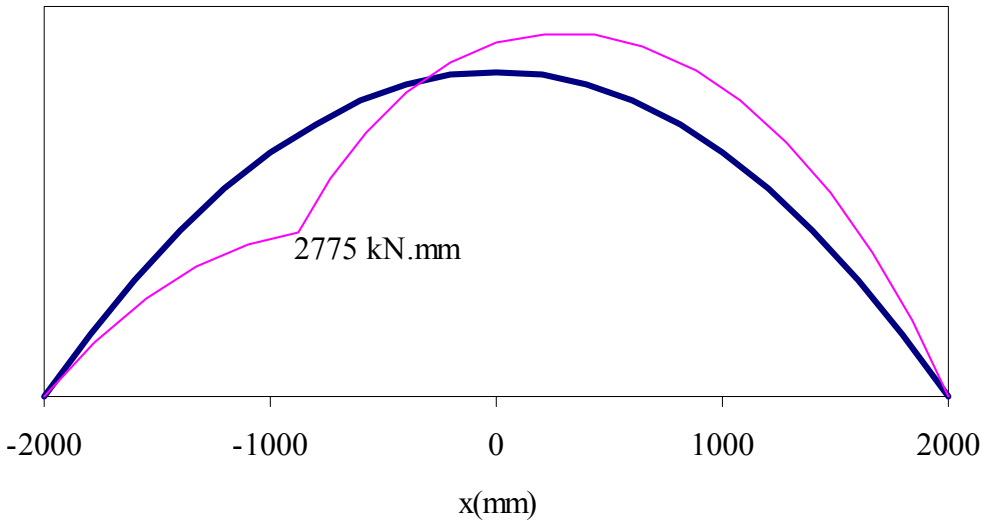

Figure A.6 – Bending moment diagram for vault 5

Azurém, P – 4800-058 Guimarães
Tel. +351 253 510200 • Fax +351 253 510217

ANNEX B

N-M Interaction Diagrams for the Vault Series

Here, each *N-M* interaction diagram constructed for the cross section of the arch is given, together with the value of Mp_1 for ultimate load, obtained using the iterative process for the plastic analysis.

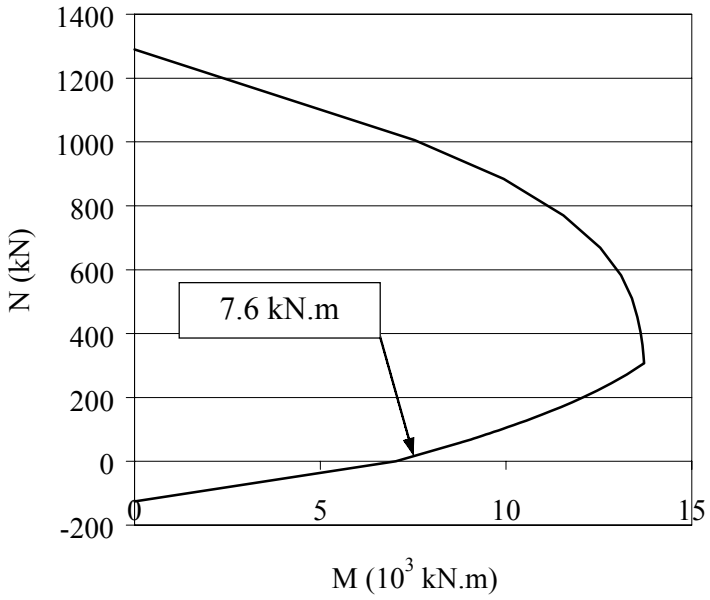

(a)

Azurém, P – 4800-058 Guimarães Tel. +351 253 510200 • Fax +351 253 510217

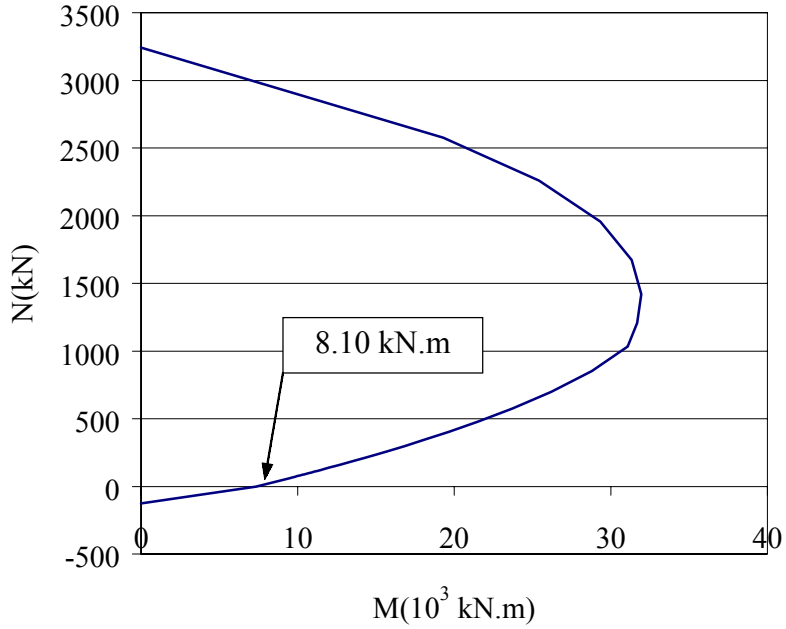

(b)

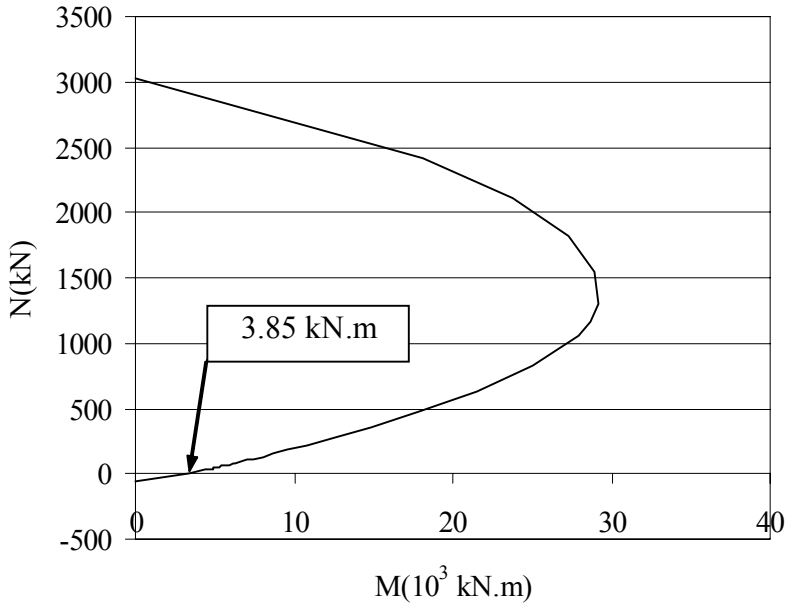

(c)

Azurém, P – 4800-058 Guimarães
Tel. +351 253 510200 • Fax +351 253 510217

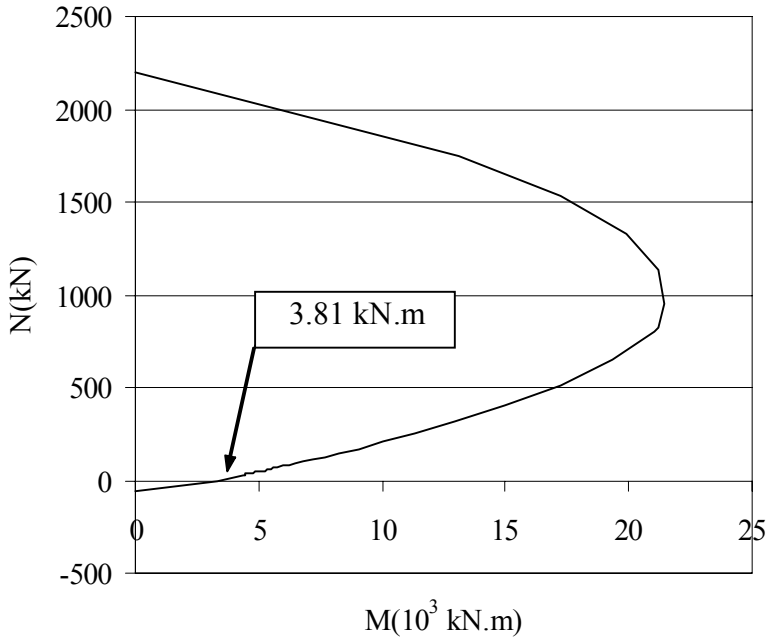

(d)

Figure B.1 – N-M interaction diagram and Mp_1 value for the maximum plastic load for vault series: a) 1 / 2; b) 3; c) 4; and d) 5.

Azurém, P – 4800-058 Guimarães Tel. +351 253 510200 • Fax +351 253 510217

ANNEX C

Plastic Design Results for the Consideration of f_{tm}=0 and Mp_2=0

(a)

Iter	x_2 (mm)	P^p_u (kN)	N_1 (kN)	N_2 (kN)	Mp_1 (kN.m)	Mp_2 (kN.m)	R (%)
1	828	6.68	-9.26	-7.66	7.31	0.09	100
2	1701	13.80	-15.43	-12.55	7.49	0.15	76.63
3	1633	14.40	-15.95	-12.91	7.51	0.15	4.14
4	1629	14.44	-15.99	-12.94	7.51	0.15	0.32

(b)

Iter	x_2 (mm)	P^p_u (kN)	N_1 (kN)	N_2 (kN)	Mp_1 (kN.m)	Mp_2 (kN.m)	R (%)
1	816	11.65	-13.57	-10.86	7.82	0.13	100.00
2	1657	14.95	-16.43	-13.26	7.92	0.16	22.05
3	1628	15.24	-16.68	-13.43	7.93	0.16	1.88
4	1626	15.26	-16.70	-13.44	7.93	0.16	0.16

(c)

Iter	x_2 (mm)	P^p_u (kN)	N_1 (kN)	N_2 (kN)	Mp_1 (kN.m)	Mp_2 (kN.m)	R (%)
1	800	10.76	-12.79	-10.27	3.82	0.13	100.00
2	1543	7.54	-10.00	-8.61	3.71	0.10	29.92
3	1571	7.26	-9.76	-8.46	3.70	0.10	3.63
4	1574	7.24	-9.74	-8.44	3.70	0.10	0.33

(d)

Iter	x_2 (mm)	P^p_u (kN)	N_1 (kN)	N_2 (kN)	Mp_1 (kN.m)	Mp_2 (kN.m)	R (%)
1	812	9.13	-11.38	-9.23	3.82	0.11	100.00
2	1560	7.36	-9.84	-8.51	3.69	0.10	19.42
3	1572	7.21	-9.71	-8.42	3.68	0.10	2.04
4	1574	7.20	-9.70	-8.42	3.68	0.10	0.18

Table C.1 – Plastic design results considering f_{tm}=0 for vault: (a) 1 / 2; (b) 3; (c) 4; and (d) 5.

Azurém, P – 4800-058 Guimarães Tel. +351 253 510200 • Fax +351 253 510217

(a)

Iter	x_2 (mm)	P^p_u (kN)	N_1 (kN)	N_2 (kN)	Mp_1 (kN.m)	Mp_2 (kN.m)	R (%)
1	828	6.68	-9.26	-7.66	7.31	0.09	100.00
2	1701	13.80	-15.43	-12.55	7.49	0.15	76.63
3	1633	14.34	-15.95	-12.91	7.51	0.15	4.14
4	1629	14.44	-15.99	-12.94	7.51	0.15	0.32

(b)

Iter	x_2 (mm)	P^p_u (kN)	N_1 (kN)	N_2 (kN)	Mp_1 (kN.m)	Mp_2 (kN.m)	R (%)
1	816	11.65	-13.57	-10.86	7.82	0	100.00
2	816	16.17	-17.49	-13.78	7.96	0	27.91
3	816	16.45	-17.73	-13.96	7.96	0	1.70
4	816	16.47	-17.75	-13.97	7.96	0	0.11

(c)

Iter	x_2 (mm)	P^p_u (kN)	N_1 (kN)	N_2 (kN)	Mp_1 (kN.m)	Mp_2 (kN.m)	R (%)
1	800	10.76	-12.79	-10.27	3.82	0	100
2	800	7.91	-10.33	-8.44	3.73	0	26.44
3	800	7.73	-10.16	-8.32	3.72	0	2.35
4	800	7.72	-10.15	-8.31	3.72	0	0.16

(d)

Iter	x_2 (mm)	P^p_u (kN)	N_1 (kN)	N_2 (kN)	Mp_1 (kN.m)	Mp_2 (kN.m)	R (%)
1	812	9.13	-11.38	-9.23	3.82	0	100.00
2	812	7.74	-10.18	-8.34	3.70	0	15.21
3	812	7.65	-10.10	-8.28	3.70	0	1.15
4	812	7.65	-10.10	-8.28	3.70	0	0.07

Table C.2 – Plastic design results considering Mp_2=0 for vault: (a) 1 / 2; (b) 3; (c) 4; and (d) 5.

Azurém, P – 4800-058 Guimarães Tel. +351 253 510200 • Fax +351 253 510217